SEDIMENTOLOGY the journal of the International Association of Sedimentologists

Sedimentology (2022) **69**, 1675–1704 doi: 10.1111/sed.12968

The erosionally confined to emergent transition in a slope-derived blocky mass-transport deposit interacting with a turbidite substrate, Ventimiglia Flysch Formation (Grès d'Annot System, north-west Italy)

MATTIA MARINI* , MARCO PATACCI† , FABRIZIO FELLETTI*, ALESSANDRO DECARLIS‡,§ and WILLIAM MCCAFFREY†

**Department of Earth Science 'Ardito Desio', Università degli Studi di Milano, Via Luigi Mangiagalli 34, Milan, 20133, Italy (E-mail: mattia.marini@unimi.it)*

†School of Earth and Environment, University of Leeds, Leeds, LS2 9JT, United Kingdom

‡Department of Earth Sciences, Khalifa University of Science and Technology, PO Box 2533, Abu Dhabi, UAE

§Research and Innovation Center on CO2 and H2 (RICH), Khalifa University of Science and Technology, PO 127788, Abu Dhabi, UAE

Associate Editor – Victoria Valdez

ABSTRACT

Basal interaction beneath frontally-emergent mass-transport deposits has been widely documented in seismic data, but its effect on deposit heterogeneity not convincingly calibrated at outcrop. Several blocky mass-transport deposits occur as part of the Late Eocene Ventimiglia Flysch of north-west Italy, comprising slope-derived marlstones, representing the original slide, and turbidite material, entrained after erosion of substrate sediments; this study reports on the best exposed. Correlation of twenty-nine sedimentary logs tied to the hosting turbidite stratigraphy allows thickness and facies changes to be tracked over an area of *ca* 40 km^2, spanning the erosionally confined to emergent transition. A basal erosion >55 m deep and several kilometres wide confines a marlstone megabreccia containing megaclasts of up to 1 km across, interpreted as the product of a submarine slide originated from a sector collapse of the western basinal slope. Approaching the downstream limit of this erosional confinement the marlstone megabreccia is replaced by highly deformed turbidites that, more distally, are in turn superseded by a debrite composed dominantly of turbidite material. Structural and textural characteristics suggest that the distally-extending debrite was deposited by a forerunner debris flow formed as substrate sediments liquefied ahead of the advancing slide, whereas the deformed turbidites were accumulated at slide margins shortly before it came to a halt. Farther downstream, the debrite is a few metres thick and sits onto the undisturbed basin floor, indicating that the mass flow became emergent distally, and was sufficiently mobile (with an estimated runout in excess of a few tens of kilometres) to redistribute the material evacuated from the basal erosion (>0.5 km^3). The mass-transport deposit terminates upward into a graded marlstone conglomerate deposited by a late-stage multiphase flow. This study provides a rare insight into facies variation in a frontally-emergent mass-transport deposit, showing how basal interaction with poorly consolidated substrates can result in erosional confinement and significant transformation of the parental flow.

Keywords Basal interaction, flow transformation, mass transport deposit, slide, debris flow, substrate erosion.

INTRODUCTION

Subaqueous mass-transport deposits (MTD) and mass-transport complexes (MTC) are generally mounded features comprising sediments and/or rocks that have been remobilized *en masse* by gravity (Weimer & Slatt, 2004; Posamentier & Martinsen, 2011), having been evacuated from an up-dip source area or scar (McAdoo *et al.*, 2000; Posamentier & Martinsen, 2011). They are usually deposited either on or adjacent to slopes in seas, oceans (Camerlenghi *et al.*, 2010; Moscardelli & Wood, 2015) and lakes (Wiemer *et al.*, 2015; Zhang *et al.*, 2016; Moernaut *et al.*, 2017).

The term MTD is used in outcrop studies to refer to the sedimentary product of one single depositional event, but which may contain more than one flow phase (Payros *et al.*, 1999; Martín-Merino *et al.*, 2014; Fallgatter *et al.*, 2017). Conversely, the term MTC is commonly used in seismic interpretation when there is evidence of several MTDs but these cannot be clearly distinguished from one another (Weimer & Slatt, 2004).

Mass-transport deposits are said to be frontally-confined or frontally-emergent, depending on whether the remobilized material is contained within its scar or emerges partly or fully from it, respectively (Frey-Martínez *et al.*, 2006). The failed material can range from loose sediments with various degrees of consolidation and cohesion (Nygard *et al.*, 2002; Haflidason *et al.*, 2004; Sawyer *et al.*, 2012; Ikari & Kopf, 2015) to assemblages of solid rock clasts (Joanne *et al.*, 2013; Principaud *et al.*, 2015; Puga-Bernabeu *et al.*, 2017). As a result, upon initiation of mass wasting the remobilized material may exhibit very different rheology. It can move downslope as a coherent mass, either with very minor internal deformation (as a slide) or with considerable plastic deformation (slump), or as a non-cohesive to cohesive incoherent assemblage of particles of varying size (debris flow) (Nemec, 1990; Moscardelli & Wood, 2008; Nelson *et al.*, 2011; Shanmugam & Wang, 2015). Significant rheological changes can occur within the parental mass flow along its pathway. These changes reflect a combination of several factors (for example, composition and size of the failed mass, slope angle and gradient changes, ingestion of ambient water, entrainment of substrate material, etc.) and can explain the observed variety of MTD shapes and sedimentary architectures (Camerlenghi *et al.*, 2010; Posamentier & Martinsen, 2011; Moscardelli & Wood, 2015). In frontally-emergent MTDs, interactions with the substrate can represent a major control on parental flow transformations. In fact, substrate material can be entrained in a number of ways (for example, by resuspension, delamination, and by bulldozing) as the failed mass emerges from its scar and translates over poorly consolidated near-seafloor sediments, contributing to compositional changes, flow bulking and generation of more mobile flow types (Martinsen, 1994; Gee *et al.*, 2006; Georgiopoulou *et al.*, 2010; Posamentier & Martinsen, 2011; Shanmugam & Wang, 2015).

The basal contact of frontally-emergent MTDs and the mechanics of their interaction with the underlying sediments were recently investigated by Sobiesiak *et al.* (2018), who distinguished free-slip and no-slip mass flows. Free-slip flows override the substrate with little or no interaction owing to a range of different mechanisms (i.e. hydroplaning, shear wetting and substrate liquefaction). These effectively detach the mass-transported material from the substrate so to prevent shear stress transmission and thus ultimately to prevent widespread erosion. Conversely, the mass flow may be coupled to the substrate, which is thus variably entrained depending on the balance of the applied stress and the vertical profile of near-seafloor sediment yield strength.

Published outcrop (Payros *et al.*, 1999; Callot *et al.*, 2008; Alves & Lourenço, 2010; Amerman *et al.*, 2011; Martín-Merino *et al.*, 2014; Mulder & Etienne, 2014; Ogata *et al.*, 2014; Sobiesiak *et al.*, 2016, 2018; Fallgatter *et al.*, 2017; Payros & Pujalte, 2019; Cardona *et al.*, 2020; de Lima Rodrigues *et al.*, 2020) and subsurface examples (Bryn *et al.*, 2005; Gee *et al.*, 2006; Tripsanas *et al.*, 2008; Sawyer *et al.*, 2009; Georgiopoulou *et al.*, 2010; Mosher *et al.*, 2010; Joanne *et al.*, 2013; Miramontes *et al.*, 2016; Biancardi *et al.*, 2020) where co-genetic slide, debris flow and particulate suspension deposits can be linked

along their flow pathway have been provided from very different sedimentary contexts. Nevertheless, the evolution of the parent flows of MTDs is still poorly constrained, and so is the role of flow-substrate interactions in the development of these same MTDs.

The aim of this paper is three-fold: (i) to document the geometry and sedimentary facies partitioning of a frontally-emergent MTD interacting with a turbidite substrate; (ii) to assess likely scales of seafloor erosion and runout of the mass flow; and (iii) to better understand the effects of substrate interaction on the spatio-temporal evolution of similar MTDs. This is accomplished by detailing the sedimentary architecture of the best exposed of several MTDs found as part of the turbidite infill (i.e. the Ventimiglia Flysch) of the deep-water Roya Basin of north-west Italy (part of the greater Grès d'Annot System of south-east France). The preserved part of the MTD is up to *ca* 60 m thick and can be correlated for *ca* 7 km both parallel and orthogonal to the inferred emplacement direction. Because of its marly composition, the original slide material can be clearly distinguished from the siliciclastic turbidites entrained from the basin floor. Correlation of twenty-nine sedimentary logs (tied to the turbidite stratigraphy below and above), suggests deposition after one single mass wasting event, and allows both an area of erosional confinement, infilled by a marlstone megabreccia, and a distal emergent deposit with hybrid composition to be defined. The study provides unprecedented detailed insights into sedimentary facies trends that can be used to constrain the spatio-temporal evolution of frontally-emergent submarine slides as they transition from being confined within their sole erosion to being emergent distally.

GEOLOGICAL SETTING

The study area is located inland of the town of Ventimiglia, Italy (Fig. 1), and is part of the Eocene fill of the foreland basin of the south-western Alps (Dallagiovanna *et al.*, 2017). Here, Cenozoic rocks unconformably overlay the thick sedimentary succession of Mesozoic carbonates and subsidiary lithologies accumulated onto the margin of the European plate (Graciansky *et al.*, 2011; Decarlis *et al.*, 2013, 2014). The latter include late Triassic shallow water carbonates and evaporites (Fig. 2A), which have been subject to halokinesis since the early Jurassic, thereby acting as a major local control on both sedimentation and tectonics (Dardeau & Graciansky, 1990; Decarlis *et al.*, 2014; Fig. 2B).

Following the continental collision between Africa and Europe the study area was involved in the forebulge of the foreland basin system of the western Alps and uplifted in the early

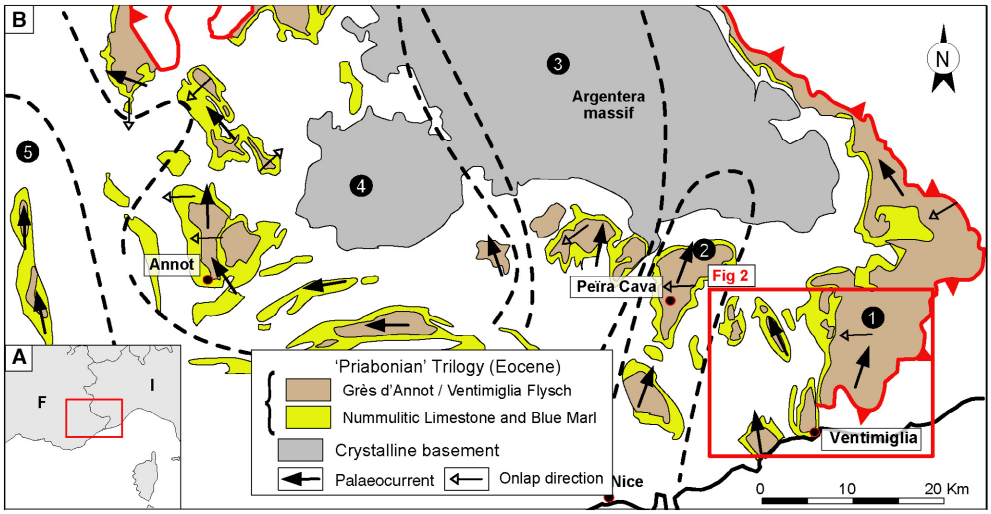

Fig. 1. Main outcrops of turbidites interpreted as the infill of sub-basins belonging to the greater Grès d'Annot turbidite system. The location of the study area, detailed in Fig. 2, is highlighted by the red rectangle. Sub-basins legend: 1 – Roya; 2 – Contes–Peïra Cava; 3 – Mont Tournairet; 4 – Quatre Cantons–Sanguinière and Main Annot; 5 – Barrême. Redrawn, after Joseph & Lomas (2004).

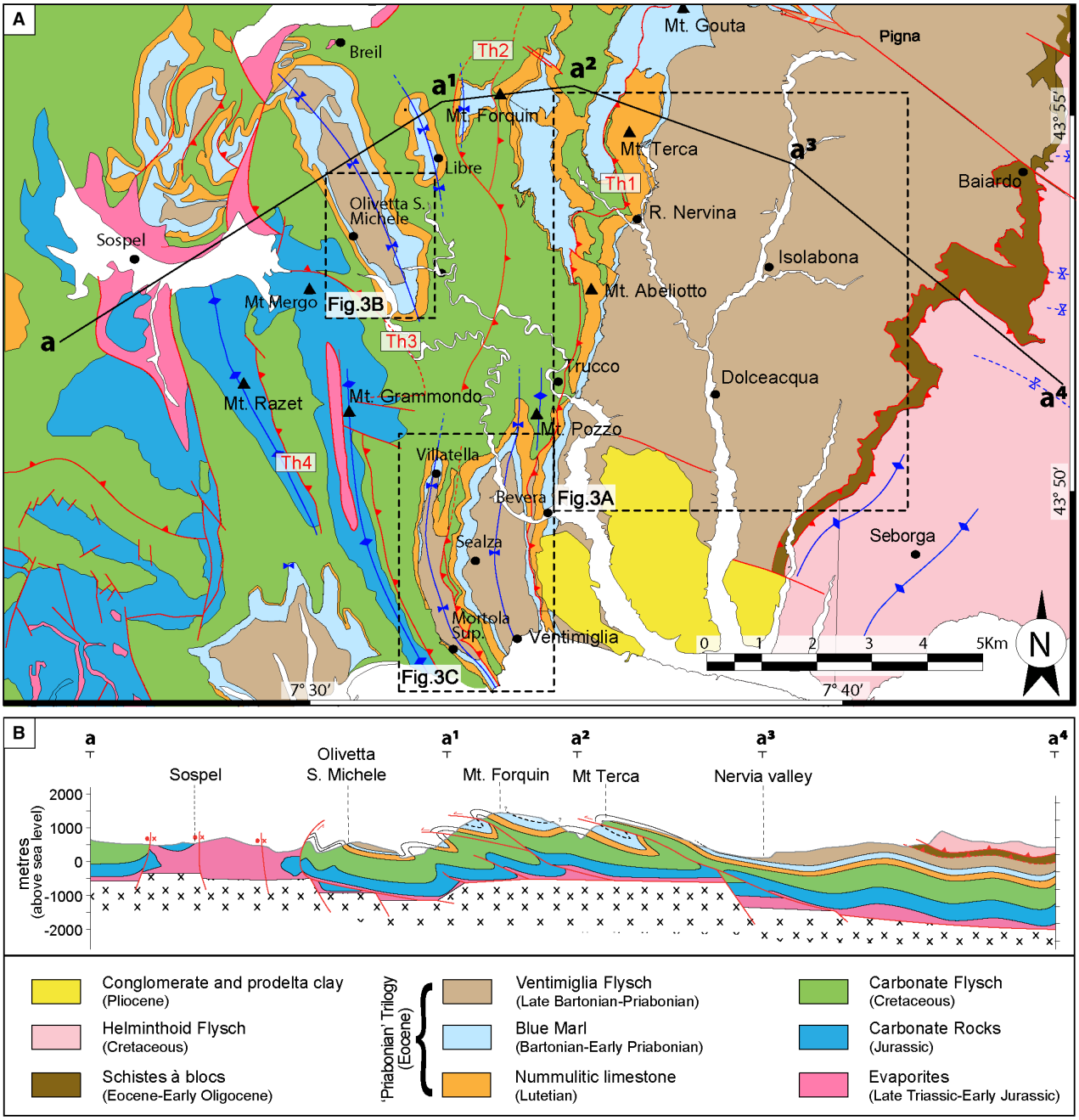

Fig. 2. (A) Simplified geological map of the study area (see Fig. 1 for location) and (B) geological cross-section. Note how the Triassic evaporites act as a decollement layer for thrusts and are locally thickened (for example, Sospel), suggesting previous halokinesis. Modified, after Decarlis *et al.* (2014).

Palaeogene, which resulted in widespread erosion and consequent formation of the top Cretaceous unconformity (Campredon & Giannerini, 1982; Apps *et al.*, 2004; Graciansky *et al.*, 2011). From the early Eocene, tectonic loading by Alpine thrust sheets led to subsidence, with deposition of a characteristic tripartite lithostratigraphic sequence (Fig. 1), which is widespread in the western Alps (the 'Priabonian Trilogy' of Boussac, 1912) but diachronous, becoming younger westward due to migration of the Alpine thrust front. This trilogy comprises a basal limestone, a middle marlstone interval and an upper succession of siliciclastic turbidites (Fig. 1).

The basal limestone (Nummulitic Limestone hereafter; *cf.* Calcareniti di Capo Mortola of Gianmarino *et al.*, 2010; Dallagiovanna *et al.*, 2017) was deposited as a relatively shallow carbonate ramp, later drowned as subsidence continued (Sinclair, 1997). As a result, an epibathyal to bathyal environment (water depths in the range 500 to 1000 m; Dallagiovanna *et al.*, 2017) was established with the deposition of up to 300 m of dominantly hemipelagic marlstones (Blue Marl hereafter; Bartonian – early Priabonian; Campredon, 1972; Mougin, 1978; Charollois *et al.*, 1980).

In the study area, the Blue Marl (*cf.* the Olivetta San Michele silty marlstones of Gianmarino *et al.*, 2010; Dallagiovanna *et al.*, 2017) initiates with a few tens of metres of thin-bedded alternations of marlstones and calcareous marlstones but are volumetrically dominated by medium to thick-bedded structureless calcareous marlstones and silty marlstones, in which the siliciclastic component (mainly quartz, muscovite and, more rarely, glauconite) increases up-section (Bodelle *et al.*, 1971). These are typically prone to conchoidal fracturing, and further develop a knobby appearance when weathered. Towards the top, the marlstones become increasingly intercalated with thin-bedded fine-grained siliciclastic turbidites (*cf.* Marnes Brunes Inferieur; Stanbrook & Clark, 2004), interpreted to represent the distal/lateral fringes of the Ventimiglia Flysch turbidite system. In the study area, the biostratigraphic age of the top of the Blue Marl (and thus of the onset of the Ventimiglia Flysch) varies from late Bartonian in the Dolceacqua area (Fig. 3A) to early Priabonian in the Olivetta syncline (Fig. 3B), with the foraminiferal association of the Sealza and Mortola synclines (Fig. 3C) being a slightly younger age than that of the Dolceacqua area (Campredon, 1972; du Fornel *et al.*, 2004).

Deposition of the Blue Marl is followed by the onset of deep water siliciclastic sedimentation (Grès d'Annot of south-east France, called the Ventimiglia Flysch in the study area; Gianmarino *et al.*, 2010; Gianmarino *et al.*, 2010) in an axial foredeep setting (Dallagiovanna *et al.*, 2017). This turbidite unit (estimated as being up to *ca* 1000 m thick) has long been recognized as the infill of the innermost of a series of sub-basins (the Roya sub-basin of Apps, 1987; Fig. 1) hosting the deposition of the greater Grès d'Annot turbidite system (Boussac, 1912; Stanley, 1961; Sinclair, 1997; Ford *et al.*, 1999; Apps *et al.*, 2004). The Bartonian onset of deposition of the Ventimiglia Flysch is older than that of Grès d'Annot outcrops of south-east France (for example, in the Contes–Peïra Cava, Mont Tournairet, Quatre Cantons–Sanguinière, the main Grès d'Annot and Barrême; du Fornel *et al.*, 2004), whereas petrography and palaeoflow patterns (Fig. 1) indicate a common southerly sediment source, corresponding to the Corsica–Sardinia block, supplemented by the Maures–Esterel massif (Jean *et al.*, 1985; Apps, 1987; Joseph & Lomas, 2004).

The Ventimiglia Flysch crops out in a largely monoclinal, north-west-dipping structural element in the east of the study area and in the hanging-wall of thrust Th1 (Figs 2A and 3A; hereafter called 'Dolceacqua–Olivastro structural element'), and in a series of westerly outliers at the core of partially overturned synclines (Figs 1C and 2B). Oligocene–Miocene contractional tectonics (Decarlis *et al.*, 2014) and contrasting turbidite facies associations make it difficult to establish the original relationship between the stratigraphic intervals preserved in the different structural elements.

The westward younging of the base of the Ventimiglia Flysch (Campredon, 1972; du Fornel *et al.*, 2004) may indicate a simple progressive lateral onlap onto a roughly north–south striking foreland ramp (Ravenne *et al.*, 1987; Joseph & Lomas, 2004), which is in agreement with sole structures in turbidites running parallel to its strike (Kneller & McCaffrey, 1999). However, the western bounding slope likely had a more complex profile, potentially hosting perched accommodation space, as suggested by thickness changes in the Nummulitic Limestone and the Blue Marl (Franchi, 1926; Campredon, 1972; Decarlis *et al.*, 2014; Dallagiovanna *et al.*, 2017), with the latter absent at a few localities, such as Bevera, Villatella and Mortola (Campredon, 1972). Although Campredon (1972) interpreted these variations as related to tectonic deformation, they were later recognized to reflect the presence of palaeotopographic highs linked to halokinesis of Triassic evaporites (for example, the Trucco and Grammondo highs; see Decarlis *et al.*, 2014). Similar thickness variations in pre-turbiditic units have been documented elsewhere in the greater Grès d'Annot system and there interpreted to reflect the development of pre-depositional and syn-depositional topography related to active tectonics (Elliott *et al.*, 1985; Apps *et al.*, 2004). Thus, the westerly outliers of the Ventimiglia Flysch (Olivetta San Michele, Mortola and Sealza synclines) might represent remnants of a late stage fill of distinct depocentres, when relatively small north–south troughs perched high on the main basin western slopes were finally supplied with siliciclastic sediment.

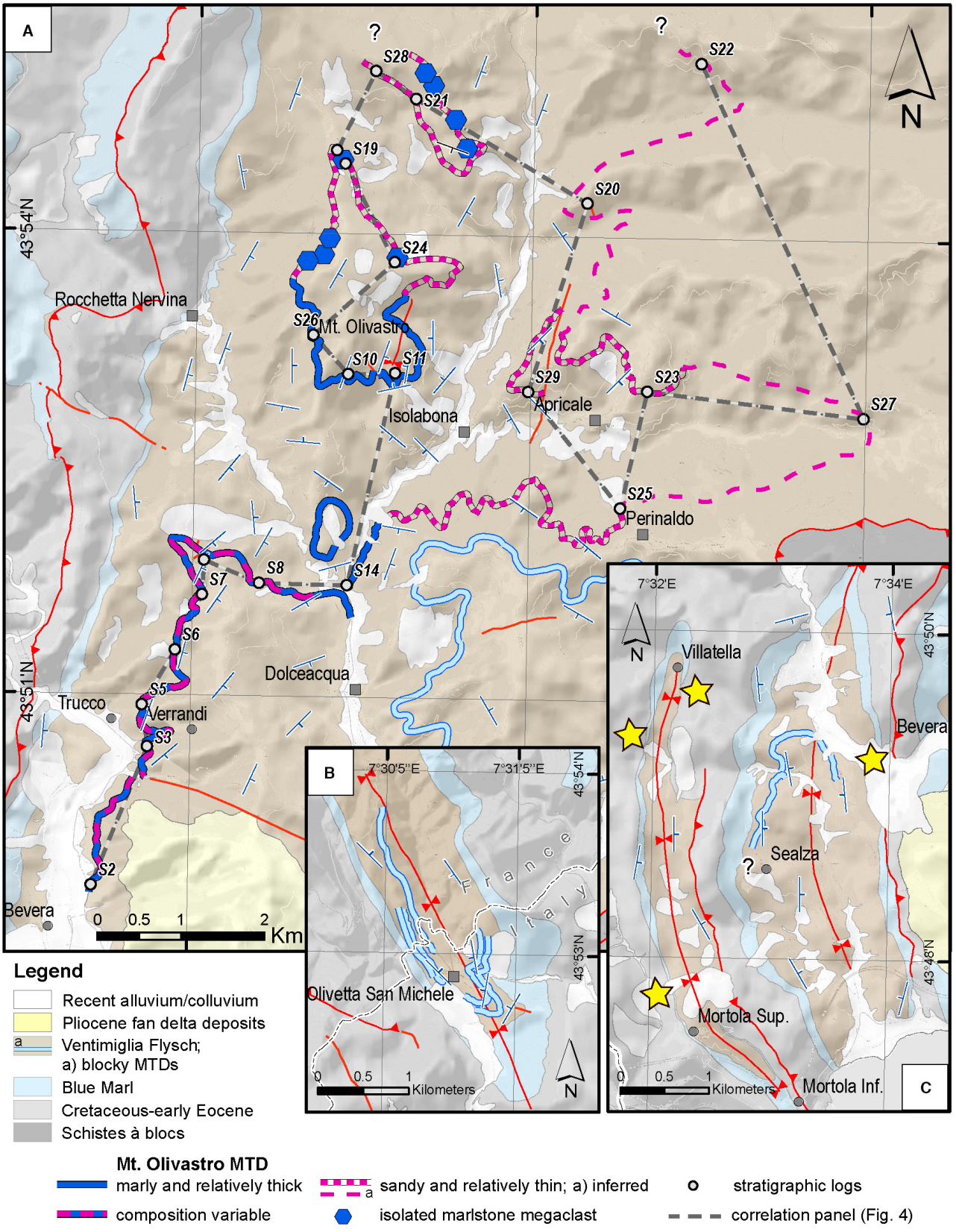

Fig. 3. (A) Simplified geological maps (modified, after Decarlis *et al.*, 2014; see Fig. 2B for location) of the main outcrop and the outliers of the Ventimiglia Flysch at the core of (B) the Olivetta San Michele syncline and (C) the Mortola and Sealza synclines with occurrence of mass transport deposits (MTDs). In (A), locations of correlation panel and sedimentary logs of Figs 4 and 9 are shown and observations on character of the Mt. Olivastro MTD summarized with different line formats (see legend). In (C) Stars indicate where the Blue Marl is locally thin or even absent in the western limb of the Mortola syncline.

A number of MTDs composed mainly of Blue Marl lithologies and with similar sedimentary facies and internal organization occur in the Ventimiglia Flysch, both in the westerly outliers and in the Dolceacqua–Olivastro structural element (Fig. 3). This study focuses on the best exposed and stratigraphically lowermost of the two MTDs documented in the Dolceacqua–Olivastro structural element (Fig. 3A); it can be followed over an area of at least 40 km^2 and is here referred to as 'Mt. Olivastro' MTD (Fig. 3).

DATA, METHODS AND TERMINOLOGY

Twenty-nine detailed stratigraphic sections of the Mt. Olivastro MTD including a few tens of metres of the encasing turbidites above and below were logged using a high-precision Jacob staff with rotatable laser (Patacci, 2016) (Figs 3A and 4). Graphical logs of the blocky part of the MTD were drawn in the field at a scale 1:100 or 1:50, according to the vertical scale of facies variability. MTD characterization included description of lithology (for example, marlstone versus turbidite sandstone and mudstones), size, shape and internal character of component elements, including strain indicators, where present. Based on these observations, logged MTD intervals were classified into six facies (*MTD facies* section). The turbidites were measured at centimetre-scale resolution and the logs drawn in the field at 1:50 scale, making note of sedimentary structures and orientation of palaeoflow indicators, where present. The grain-size and textural description approach of Blair & McPherson (1999) was adopted, which extends the Udden-Wentworth scale and adapts previous classification schemes to deposits containing clasts larger than 4.1 m. Following these authors, clasts larger than 4.1 m will be referred to as megaclasts, which can be further distinguished into blocks (from 4.1 to 65.5 m), slabs (from 65.5 to 1048.6 m), and kilometre-scale monoliths (from 1.0 to 33.6 km) and megaliths (above 33.6 km). Accordingly, the term megabreccia will be used to refer to a deposit made of chiefly angular megaclasts.

Selection of key sections and dataset interpretation was informed by GIS software-aided mapping of the marlstone-prone parts of the MTD (Fig. 3A), which can be easily distinguished on satellite images owing to their lighter colour and their tendency to form relatively un-vegetated terrain.

Since multiple lines of evidence suggest that the observed part of the Mt. Olivastro MTD had a relatively flat top (*MTD geometry and sedimentary facies partitioning* section), the upper MTD surface was used as a datum on which to flatten sedimentary logs (Fig. 4).

In this work, the term 'substrate' is used to refer to the turbidites below the MTD that, even though mildly deformed locally, occur at the same stratigraphic height in multiple sections (Fig. 4), suggesting that they have not been moved from their original position. Since the Mt. Olivastro MTD is chiefly composed of extrabasinal clasts derived from mass wasting of the Blue Marl, the term 'hybrid' is used to refer to those parts of the deposit that include turbidite material entrained from the substrate. The base of the MTD is identified as the interface separating the substrate from materials carried by mass-transport processes, which thus represents both the sliding surfaces onto which the mass flows travelled before coming to a halt, as well as the lower boundary of substrate erosion. In the more distal outcrops there is evidence of only very minor erosion (for example, logs S22 and S27 in Fig. 4). Therefore, the top of the youngest turbidite event bed below the MTD is assumed to best approximate the pre-MTD basin floor ('inferred basin floor', hereafter). Thus, the 'depth of erosion' (*Megabreccia* section) has been calculated as the (undecompacted) stratigraphic thickness between the base of the MTD and the inferred basin floor.

RESULTS

Turbidites

An extensive description of the sedimentary facies of the turbidites below and above the Mt. Olivastro MTD is beyond the aim of this paper.

Nonetheless, correlations and palaeoflow indicators in the turbidites encasing the MTD (Fig. 4) provide important constraints on MTD geometry. Overall, the Ventimiglia Flysch turbidites encasing the Mt. Olivastro MTD show a sheet-like architecture with thick mudstone caps suggestive of a confined basin floor setting (Pickering & Hiscott, 1985) and therefore provide excellent tabular markers to help establish the MTD geometry (*MTD geometry and sedimentary facies partitioning* section).

The turbidites below and above the MTD show similar sedimentary facies and stratal patterns, with packages of thin-bedded turbidites up to several metres-thick alternating with thick to very thick sandstone–mudstone co-genetic couplets. Below the MTD, four of these very thick event beds form a marker quadruplet that can be easily spotted from distance and can be followed laterally for several kilometres with only minor facies and thickness changes. Palaeoflow from sole marks is towards the NNE with very low dispersion (Fig. 4), whereas that from ripples indicates a higher variability, suggestive of interaction with basinal slopes.

The turbidite sequence above the MTD begins with a *ca* 10 m thick bed set of thin-bedded turbidites sandwiched between two distinctive very thick turbidite event beds (grey bands in Fig. 4). This sequence can be widely correlated bed-by-bed with minor variations in thickness and sedimentary facies (sand content decreases slightly towards the north). However, in a few localities this interval can be partly (logs S11 and S28; Fig. 4) or completely (log S3; Fig. 4) missing, suggesting that the MTD top was locally elevated above the basin floor, as discussed in the *MTD geometry and sedimentary facies partitioning* section. The few palaeocurrent indicators measured in the turbidites above the MTD show palaeoflow similar to that in the pre-MTD turbidites, thus suggesting that the MTD emplacement did not result in any major change in the direction of the later gravity flows.

MTD facies

Deformed turbidites

This facies consists of variably deformed turbiditic material that has been detached from the substrate and that cannot be matched with the stratigraphy below the MTD. Thickness varies from a few decimetres to a few tens of metres (Figs 4 and 5). The position of this facies is always directly above the substrate (Fig. 5A to C), with the contact occurring across a basal shear layer with highly variable thickness ranging from a few to several tens of centimetres (Fig. 5C). Placing the upper boundary is straightforward when this facies is overlain by marlstone material, but can be problematic in more distal sections (for example, S20, S23, S25 and S29; Figs 3 and 4), where it is overlain by a debrite made mostly by turbidite material (*Debrite with substrate material* section).

The style of deformation changes depending on the material involved and location. Thick-bedded turbidites tend to form horses of slightly deformed imbricated rafts (Fig. 5A). Thin-bedded packages are instead more prone to be intensely sheared with development of a block-in-matrix texture (Fig. 5B), albeit that in more easterly locations they tend to form by imbricate horses (with scales of a few to several metres) with coherent internal folding (Fig. 5C). Folds may be tight to isoclinal, overturned or event recumbent, with smaller examples representing drag folds associated with secondary shear planes (Figs 5C and D). Some folds are rootless and ptygmatic, and may have stretched limbs with pinch-and-swell structures or even sandstone *boudins* developed along them (Figs 5C and D). Where discernible, fold vergence is always towards easterly quadrants, suggesting a mean shear from above towards the east.

Interpretation: Similar deformed strata are widely documented underneath blocky MTDs (Tripsanas *et al.*, 2008; Alves & Lourenço, 2010; Ogata *et al.*, 2014; Sobiesiak *et al.*, 2018; Cardona *et al.*, 2020; Pini *et al.*, 2020) and interpreted as the product of shear within either the basal part of the moved mass (basal shear zone; e.g. Alves & Lourenço, 2010; Cardona *et al.*, 2020) or at its lateral and frontal regions (Bull *et al.*, 2009). The generally sharp, clear-cut boundary with the substrate indicates that erosion and entrainment of intrabasinal material might have focused along discrete, planar intervals of weaker stratigraphy below the basin floor. The observed pseudo-ductile deformation style of the deformed turbidites suggests that the material involved was unlithified, poorly compacted and locally prone to liquefaction. In the absence of evident folding (for example, when the scale of folding is larger than the outcrop), it can be difficult to differentiate deformed and *in situ* turbidites. A case in point occurs in log S29, where the few metres of turbidites below the MTD are only slightly deformed. Although they appear in place, there are no plausible correlations with the laterally equivalent *in situ* substrate stratigraphy of nearby

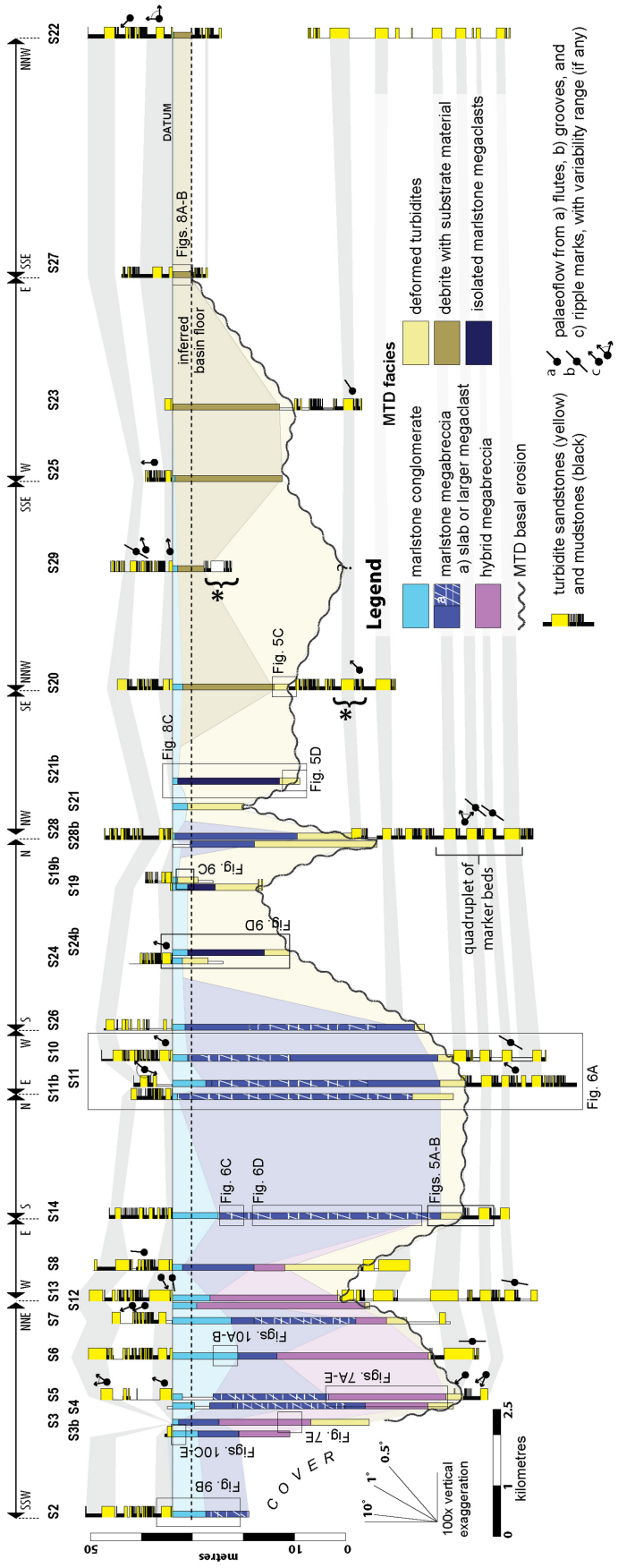

Fig. 4. Correlation panel (with 100x vertical exaggeration) illustrating the occurrence of mass transport deposit facies (see *MTD facies* section) in logged sections (see Fig. 3A for location), with reference to figures discussed in the text. Main marker beds in the turbidites below and above the MTD are highlighted in grey. Correlations were flattened to the MTD top (see *MTD geometry and sedimentary facies partitioning* section for explanation). Note how the few metres of stratigraphy below the MTD in log S20 (curly bracket and star) most likely correspond to that in the deformed turbidite of log S29.

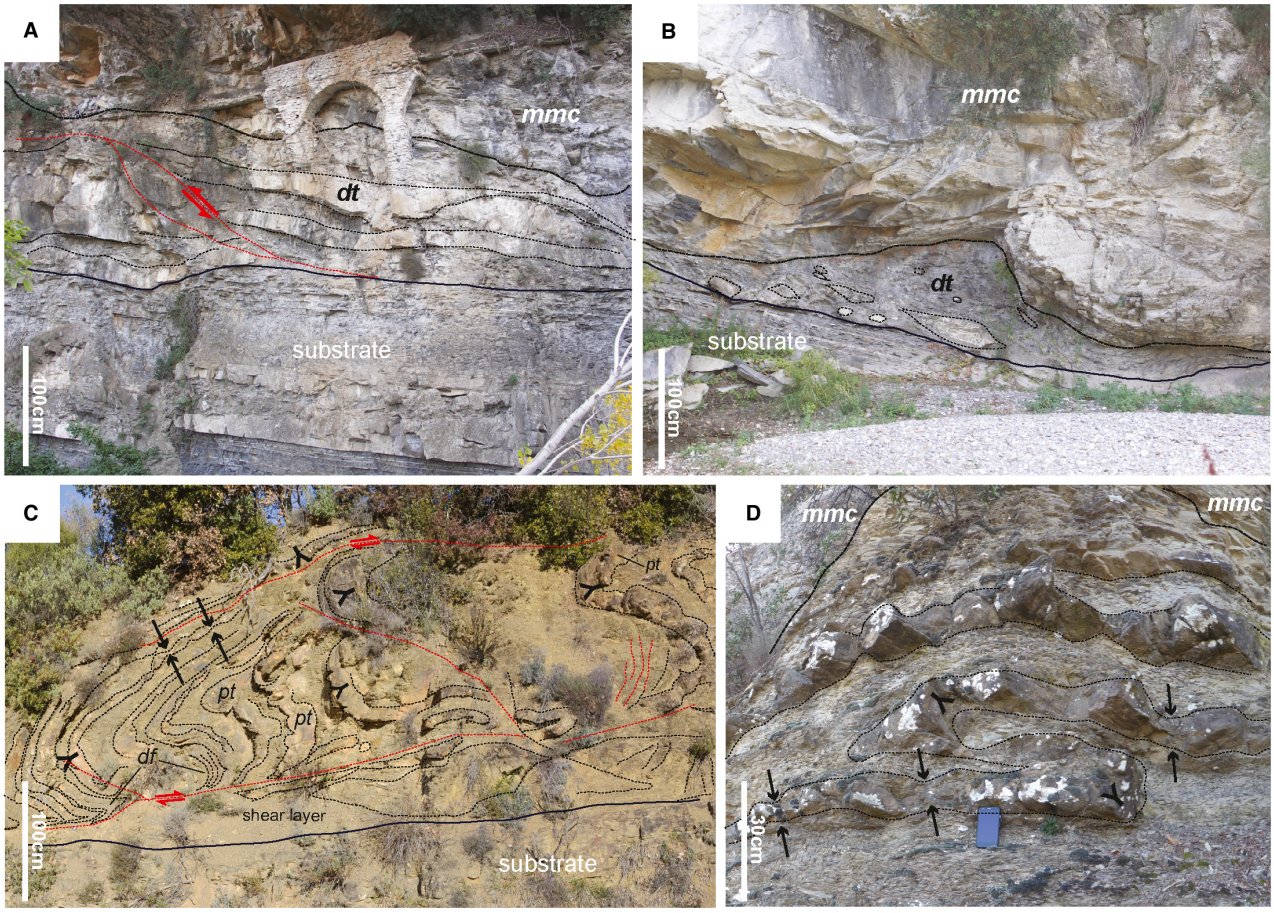

Fig. 5. (A) The deformed turbidites (*dt*) below a marlstone megaclast (*mmc*) in log S14 (see Figs 3 and 4 for location). Note the imbricated turbidite rafts, up to block size, separated from one another by shear planes (dotted red lines). (B) Detail showing the block-in-matrix texture of the deformed turbidites, made of intensely sheared sandstone clasts floating in a muddy matrix with a pseudo-foliated appearance. (C) North-looking view of the lower part of the deformed turbidites in log S20 (see Figs 3 and 4 for location) showing easterly facing recumbent similar folds (tail of Y points towards youngest strata). Note the drag folds (*df*) above the basal shear surface indicating a top to the right (east) shear sense, the presence of ptygmatic folds (*pt*), and the pinch and swell geometry of some fold limbs (arrows). (D) Recumbent folds within the deformed turbidites below a marlstone megaclast in log S21b. The axial plane plunges towards the west (away from the observer), giving a top to the east shear sense.

logs S22 and S27; rather, they may correspond to the sequence found at a deeper level in log S20 (Fig. 4; curly bracket and star). Thus, they are interpreted to be displaced, with possible vertical movement of up to 20 m.

Megabreccia

Reaching a thickness of up to *ca* 50 m (for example, S10–S11 and S4–S5; Fig. 4), this facies constitutes the main volumetric component of the observed part of the Mt. Olivastro MTD. Two types of megabreccia can be distinguished, based on composition and texture: a tightly packed marlstone megabreccia, which is virtually devoid of matrix (*Marlstone megabreccia* section) and a hybrid type composed of a mix of turbidite and marlstone boulders and a variable amount of finer-grained matrix (*Hybrid megabreccia* section). When both types of megabreccia are present, the hybrid type is restricted to the lower part of the deposit.

Marlstone megabreccia. This facies is best exposed in a *ca* 5 km long outcrop belt to the south of the Mt. Olivastro summit (Fig. 3A), in which megaclasts at least a few hundreds of metres across (slabs and potentially monoliths, *sensu* Blair & McPherson, 1999) of the Blue Marl

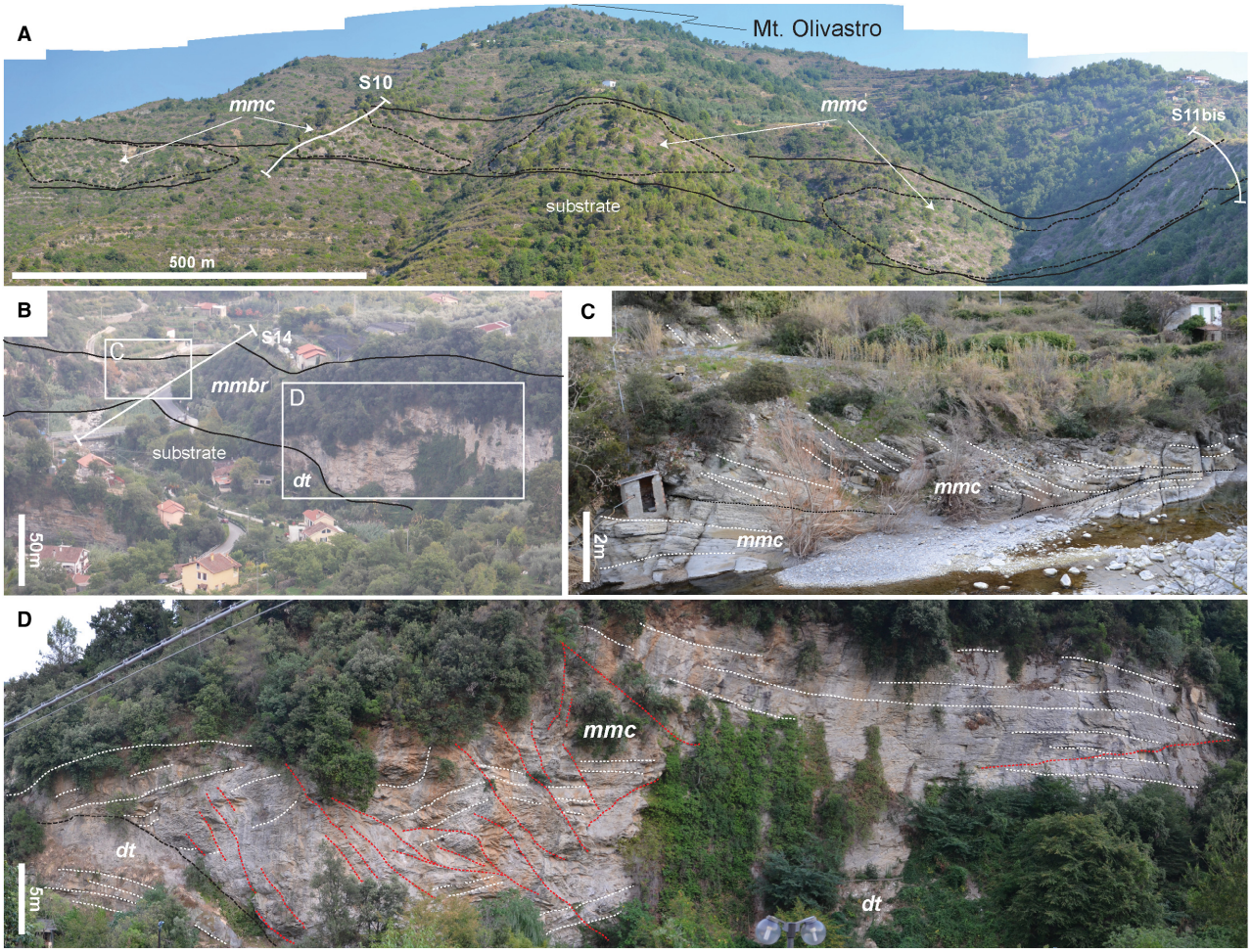

Fig. 6. (A) North-west looking view of the marlstone megabreccia at Mt. Olivastro highlighting presence of large marlstone megaclasts the size of slab or larger (*mmc*). (B) South-looking view of the marlstone megabreccia (*mmbr*) at the confluence of the Barbaira and Nervia rivers with details showing (C) welded contacts (dotted black lines) between megaclasts and (D) faults (dotted red lines) cutting the internal stratification (dashed white lines) of a marlstone slab. Note how in (D) the deformed turbidites (*dt*) below the megaclast suggest that this translated towards the left (west) shortly before coming to a halt.

alternate with areas where marlstone material crops out sparsely from the bushy vegetation (Fig. 6A). Slabs can be easily spotted from a distance, owing to their coherent internal stratification, which is generally undeformed or only slightly deformed; their apparent long axis lies parallel to internal stratification and at angles <15° from palaeohorizontal (*cf.* with facies I of Tripsanas *et al.*, 2008). In most of the logged sections, slabs float in the megabreccia, although locally they can be directly in contact with and penetrate into deformed turbidites (Figs 5A, 5B and 6D). Four such slabs up to *ca* 40 m thick and with minimum horizontal lengths in the range 100 to 250 m can be seen in the Mt. Olivastro outcrop (logs S10, S11, S11b and S26; Figs 4 and 6A); at least two more slabs of similar size occur in the Roja Valley (logs S4 and S5; Figs 3A, 4 and 5C).

However, the largest megaclast exposed at outcrop is that measured in log S14 (Figs 4 and 6A), which reaches a thickness of *ca* 40 m and show lengths in excess of *ca* 800 m horizontally. Slabs are generally poorly deformed at their core but can be cut by faults with a range of scales at their edges (Fig. 6D).

The remainder of the marlstone megabreccia comprises very coarse elongated boulders and blocks with preserved internal bedding but showing gently deformed edges and welded contacts suggestive of soft-sediment deformation

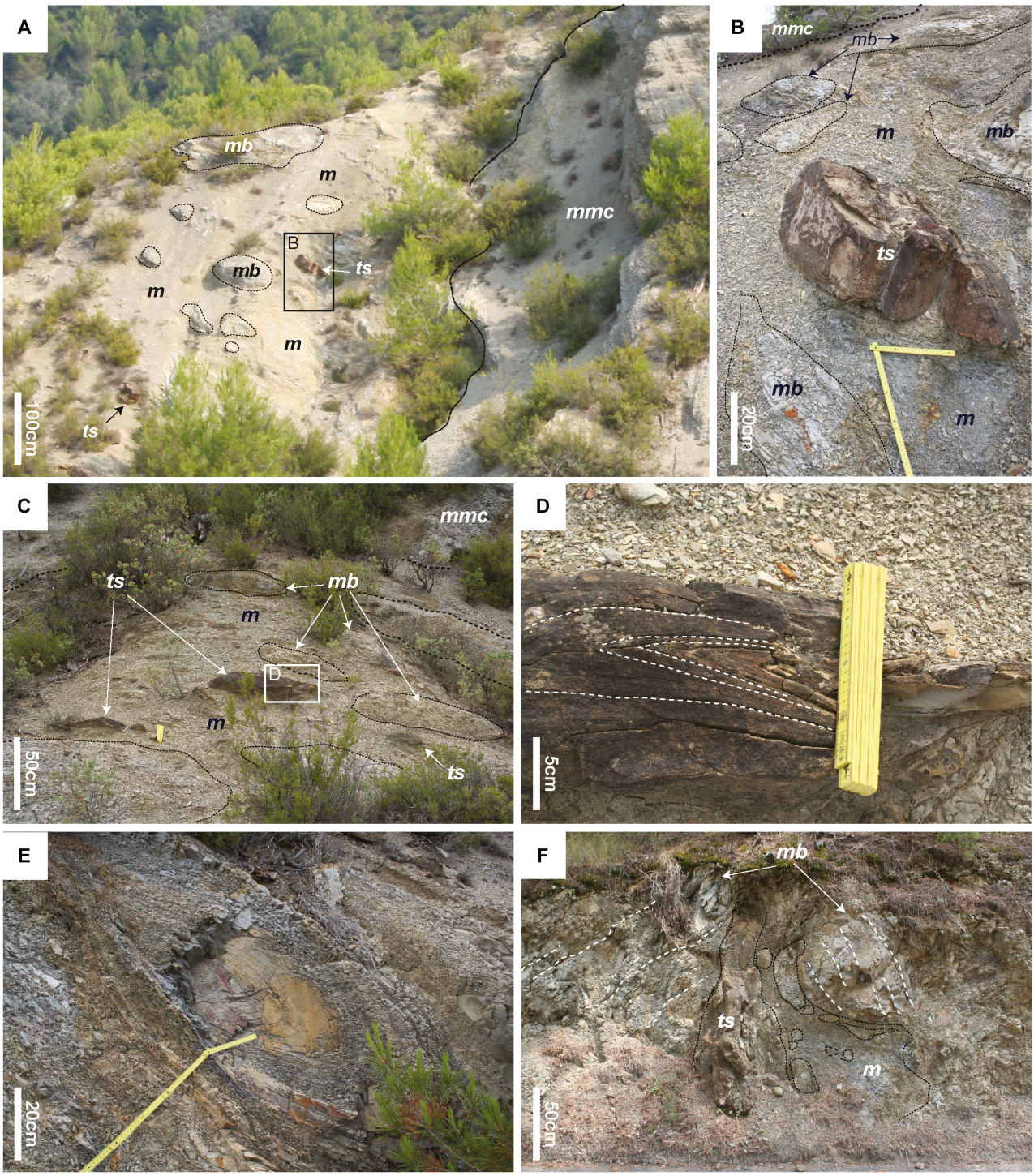

Fig. 7. (A) North-east looking view of the hybrid megabreccia underlying a marlstone megaclast (*mmc*) in log S5 (see Fig. 4 for location). Note the block-in-matrix texture made of marlstone boulders (*mb*) and blocks (*mmc*) and turbidite sandstone (*ts*) floating in a matrix (*m*) of sheared finer-grained material. Turbidite sandstone remnants show lozenge-like shapes (B) and intrafolial folds (C) and (D), indicating a top to the left (north-east) shear sense. (E) Tightly folded marlstone boulder in which the intersection of primary sedimentary layering and fracture cleavage isolate centimetre-sized rock fragments. (F) Road cut through the hybrid megabreccia of log S3 exposing marlstone and turbidite sandstone boulders, surrounded by a finer-grained and intensely sheared matrix.

(Fig. 6C). As a result, the deposit is clast supported and tightly packed, with no discernible matrix material. As per the slabs, the short axis of this clast population is generally orthogonal to the internal bedding and the angle between the internal bedding and the palaeohorizontal is generally less than 20°.

Interpretation: Although characterized by different lithologies, megaclast-bearing breccias similar to that of the Mt. Olivastro MTD are widely documented both at outcrop and in the subsurface (Tripsanas *et al.*, 2008; Alves & Lourenço, 2010; Jackson, 2011; Martín-Merino *et al.*, 2014; Alves, 2015; Gamboa & Alves, 2015; Sobiesiak *et al.*, 2019) and interpreted as deposits linked to submarine sliding of variably consolidated near-seafloor sediments. The juxtaposition of slabs and the relatively finer-grained material surrounding them (Fig. 6A) is here interpreted to reflect the fragmentation during downslope motion of what presumably was a larger coherent failed mass.

Hybrid megabreccia. This facies occurs in southerly outcrops only (logs S3–S8 and S13), sandwiched between the underlying deformed turbidites and overlying marlstone megabreccia. The hybrid megabreccia shows a block-in-matrix texture consisting of an unsorted mélange of boulders of marlstone and, subordinately, turbidite sandstones and mudstones, surrounded by a matrix of finer-grained material (Fig. 7).

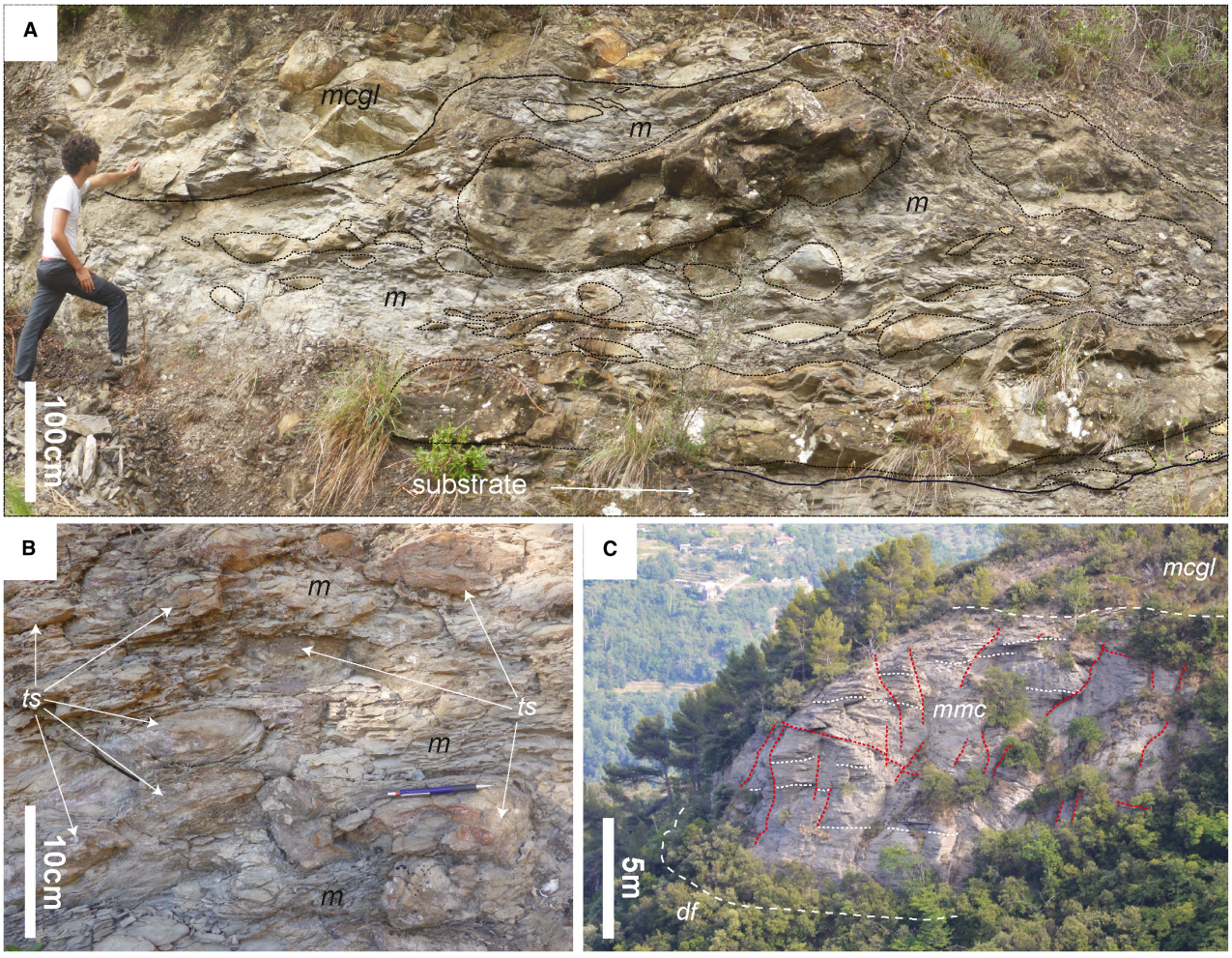

Fig. 8. (A) The debrite with substrate material in log S27 underlies the marlstone conglomerate (*mcgl*) and is composed turbidite sandstone clasts up to boulder size, floating in a siliciclastic mudstone matrix (*m*). (B) Detail of the debrite with substrate material showing intensely sheared turbidite sandstone clasts (*ts*) floating in a pseudo-foliated matrix of siliciclastic mudstone. (C) A marlstone megaclast (*mmc*) sitting atop the deformed turbidites (*df*) and overlain by the marlstone conglomerate. Note the mildly deformed internal stratigraphy of the megaclast, cut by a range of faults (dotted red lines) with small lateral continuity and throw.

Marlstone boulders can be either equant or highly elongated. Equant examples are angular to sub-angular and internally less deformed compared to elongated examples, which are often tightly folded and can show fracture cleavage (Fig. 7E). Boulders with turbidite composition represent less than 10% of boulders overall and occur most frequently as isolated rafts in the lower part of the megabreccia. Their deformational style is highly variable, with larger examples comprising thick-bedded turbidites generally featuring open folds with metre-scale wavelength, as opposed to isoclinal, often ptygmatic folds developed in smaller blocks made up of thin-bedded turbidites.

The matrix of the hybrid megabreccia can represent up to 15% of the deposit and consists of a pseudo-foliated marly mudstone containing clasts with sizes up to that of cobbles of marlstone and turbidite sandstone and mudstone, which show lozenge-like shapes (Fig. 7B) and intrafolial folds (Fig. 7C and D) suggestive of pseudo-ductile, soft-sediment deformation.

Interpretation: The hybrid megabreccia occurs always in the lower part of the MTD suggesting that it formed at the slip boundary region separating the initial mass flow from the substrate. The intense deformation, significant amount of fine-grained material, and hybrid composition of this facies imply intense shear and mixing of exotic marly material with variably consolidated turbiditic sediments entrained from the substrate.

Debrite with substrate material

This facies occurs in easterly sections only, sitting above the deformed turbidites and underlying the marlstone conglomerate described below. The deposit is chaotic and unsorted, as it is composed of cobble to boulder-sized clasts of turbiditic material and secondarily marlstones, floating in a matrix of siliciclastic mudstone (Fig. 8A and B). Composition is hybrid and varies greatly, but estimates made in the field suggest that turbidite material (including that dispersed in the matrix) represents generally more than 70% by volume, exceeding 90% in logs S22 and S27. Turbidite boulders are flat-laying rafts composed of either thick, slightly deformed sandstone beds (Fig. 8A), or thin-bedded turbidites, which instead are intensely folded and sheared. The relatively rarer marlstone boulders are typically equant and undeformed internally. The pebble to cobble-sized fraction comprises intensely deformed turbidite sandstone clasts (Fig. 8A and B) and rare angular to sub-rounded marlstone clasts that notably become more frequent upward (Fig. 8A).

On average, the debrite with substrate material contains *ca* 30% of matrix, represented by a slightly sandy siliciclastic mudstone with a pseudo-foliated appearance (Fig. 8B). In one locality (log S23), a *ca* 11 m thick marlstone megaclast (a block or larger) with undeformed horizontally-lying internal stratigraphy was found within this debrite.

Interpretation: The disorganized character of this facies suggests deposition from a relatively mobile flow of a mixture of mud, sand and debris of variable size (generally up to metre-scale blocks), capable of carrying marlstone megaclasts, likely with sizes up to that of small slabs. The mixed siliciclastic–marly composition indicates that the debris flow might have originated after mixing of exotic (marlstone) and poorly consolidated turbiditic material entrained from the substrate.

Isolated marlstone megaclasts

Marlstone megaclasts up to a few tens of metres thick and a few to several tens of metres wide can also occur in isolation (i.e. not as part of the megabreccia or within the debrite with substrate material), atop the deformed turbidites (Figs 3C and 4). The long axes of these megaclasts lie in the plane of internal bedding, which is generally parallel to that of the turbidites making the MTD substrate and thus the original seafloor. The internal stratigraphy of these megaclasts is only slightly deformed, being cut by high-angle faults with small lateral continuity and throw (Figs 8C and 9D). Three of these megaclasts (logs S19, S24b and S21b; see Figs 3A and 4 for location) were inspected, revealing that they are bounded below and laterally by the deformed turbidites (Figs 4, 5D and 8C), and are capped by the marlstone conglomerate described below (Fig. 9D).

Ratios of megaclast thickness to thickness of the deformed turbidites below is less than *ca* 4 (*cf.* with values reported in Alves & Lourenço, 2010).

Interpretation: These megaclasts are interpreted as outrunner blocks that detached from the slowing-down slide depositing the marlstone megabreccia (De Blasio *et al.*, 2006). Capping by the marlstone conglomerate suggests that the top of these megaclasts was not elevated significantly above the seafloor (see discussion in *MTD geometry and sedimentary facies partitioning*

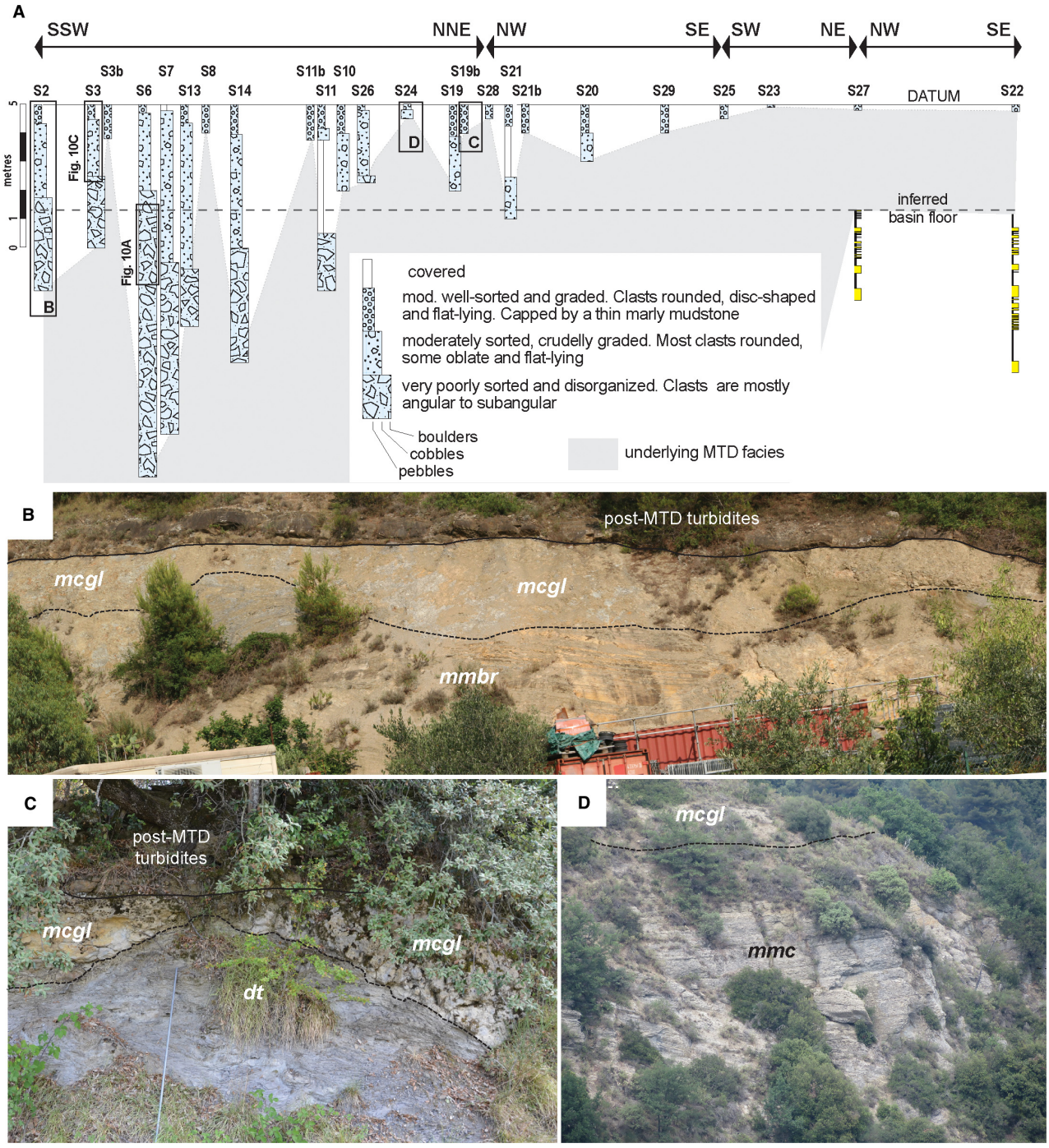

Fig. 9. (A) Correlation panel (see Fig. 3A for location) detailing the thickness and facies variability of the marlstone conglomerate in the logged sections. Note how the thickness of the conglomerate appears to compensate for the uneven top of the underlying deposits. (B) and (C) Outcrop examples of thickness changes of the marlstone conglomerate (*mcgl*) that compensate for the uneven top of marlstone megabreccia (*mmbr*) in logs S2 and of the deformed turbidites (*dt*) in log S19b, respectively. (D) The isolated marlstone megaclast (*mmc*) of log S24 is overlain by the marlstone conglomerate, suggesting its top was not associated with significant bathymetric relief.

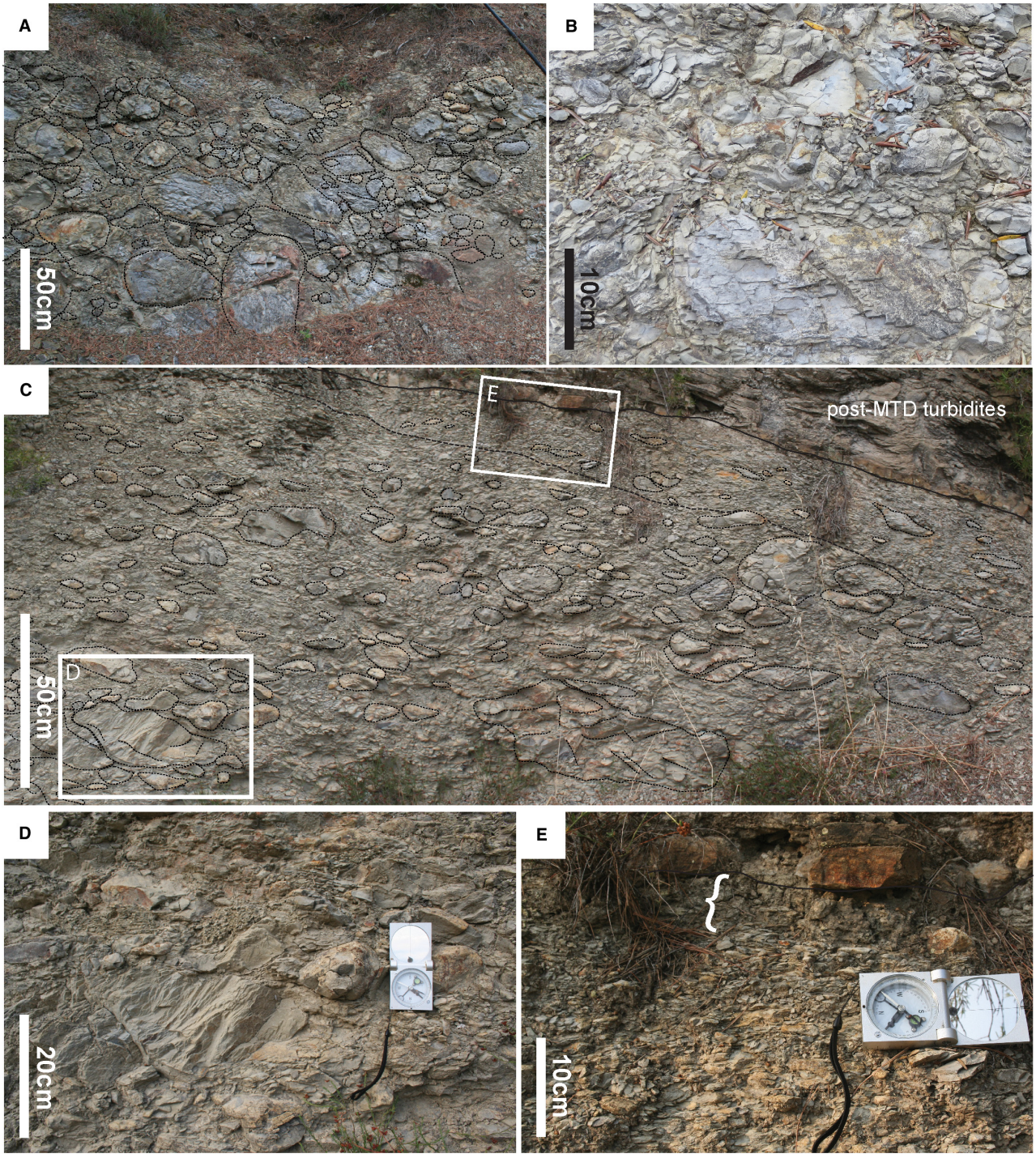

Fig. 10. (A) The very poorly sorted coarse lowermost division of the marlstone conglomerate in log S6. Note the rather disorganized texture as well as the angular shape of larger, boulder-sized clasts. (B) Detail of the lowermost division of the marlstone conglomerate in log S6 showing the densely packed structure and the presence of a range of jigsaw to conchoidal fractures. (C) The middle and uppermost divisions (below and above the black dashed line, respectively) of the marlstone conglomerate in log S3. Note the crude normal grading and the upward increase in sorting, with larger angular clasts becoming relatively less frequent towards the top. (D) Detail of a heavily fractured large marlstone cobble with jigsaw cracks. (E) The normally graded uppermost part of the marlstone conglomerate, passing upward with sharp contact to a marly mudstone cap (white curly bracket).

section). Rather, geometrical relationships indicate that, while gliding, these outrunner blocks might have foundered into the deformed turbidites.

Marlstone conglomerate

This facies constitutes the topmost part of the Mt. Olivastro MTD at all localities (Figs 4 and 9) and occurs with similar characteristics and relationship with the facies described so far in all of the MTDs mapped in the Ventimiglia Flysch (Fig. 3). It sharply overlies the deformed turbidites but has a more gradational contact with the marlstone megabreccia and the debrite with substrate material. In one MTD from the Olivetta syncline (Fig. 3B) it was found to sit directly above an undeformed turbidite substrate. This conglomerate is almost exclusively made of marlstone clasts (turbidite clasts represent <5%) together with varying proportions of marly matrix.

The thickness of the marlstone conglomerate ranges from *ca* 0.25 to 13 m and shows a first-order thinning trend towards the north-east (Fig. 9A), albeit with second-order thickness changes that are locally significant and apparently compensate for the uneven top of the underlying deposit (Fig. 9B). In the locations where this facies is thicker (for example, logs S3b, S6, S7, S13, S14 and S10) three divisions can be distinguished, based on clast size, sorting and shape (Fig. 9A). The lower division is a relatively thick clast-supported conglomerate, which is disorganized and very poorly to poorly sorted, with clasts ranging from very fine pebbles to medium boulders (Fig. 10A). Boulders are very angular to sub-angular and show evidence of brittle deformation, with a range of jigsaw to conchoidal fractures which isolate pebble to cobble-size fragments of variable size, shape, and roundness (Fig. 10A and B) similar to those infilling the space between boulders. Cementation makes it difficult to distinguish the finer-grained fraction forming the matrix, but estimates made in the field suggest that it might represent less than 10% of the deposit. Moving upward, there is a rapid transition into a finer-grained, better-organized conglomerate (Figs 9 and 10C), seemingly containing a higher (15 to 20%) fraction of muddy matrix. This division is moderately well-sorted, consisting chiefly of sub-rounded to rounded pebbles and fine cobbles with (sub-) horizontally lying oblate shape. However, typically it also contains several outsized clasts (from coarse cobbles to medium boulders; Fig. 10C), generally heavily fractured (Fig. 10D), which become less frequent upward resulting in a crude normal grading.

The uppermost division is a clast-supported pebble conglomerate a few tens of centimetres thick, with a better developed normal grading and a higher proportion of flat-lying disc-shaped pebbles and marly matrix compared to the divisions below (Fig. 10E).

Where the very top of the upper conglomerate could be observed, it is sharply overlain by a marly mudstone cap up to several centimetres thick (Figs 9C and 10E) with very rare (<5%) marlstone pebbles in its lower part.

It is noteworthy that, despite the irregular top of the deposit below (Fig. 9A and B), when sedimentary logs are flattened on the conglomerate top, the sedimentary divisions described above occur at similar stratigraphic heights all over the study area, suggesting a horizontally-lying, highly layered deposit structure.

Interpretation: The vertical organization of the marlstone conglomerate implies temporal changes in the physical character of the parent flow (Figs 9 and 10). The disorganized nature of the basal division is suggestive of rapid deposition from a non-cohesive debris flow in which particles were supported mainly by intergranular collision, whereas the increasingly better-organized and normally graded division above is suggestive of an incremental process of deposition (Mulder & Alexander, 2001; Talling *et al.*, 2012). This medial division is interpreted as the deposit of an overriding highly concentrated waning flow that, while depositing pebble-size clasts in a fast-aggrading basal layer, exerted sufficient shear stress to move large cobbles in a transient bed load layer. Lastly, the marly mudstone cap may represent the deposit of a late stage mudflow capable of entraining pebble-sized clasts from the underlying deposit. It seems likely that this interval may terminate with material deposited from suspension. As a whole, the marlstone conglomerate can be viewed as the deposit of a multiphase flow evolving from an initial debris flow into a finer-grained hyper-concentrated flow after progressive clast fragmentation and dilution by ambient water, and finally into a mudflow, likely accompanied with a highly dilute turbulent wake.

This facies shows similarities with a range of deposits reported in the literature (Sohn *et al.*, 2002; Payros *et al.*, 1999; Fallgatter *et al.*, 2017), albeit it has been rarely documented in association with slide deposits below (e.g. Tripsanas

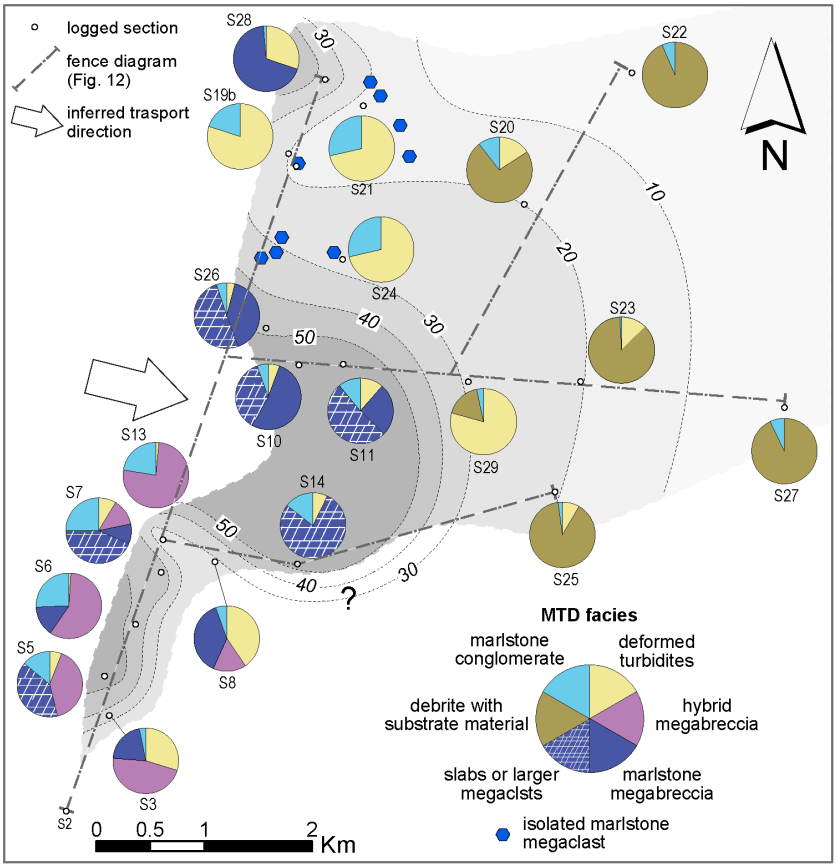

Fig. 11. Simplified interpretation of the depth (m) of the Mt. Olivastro mass transport deposit (MTD) basal erosion. Pie charts show the thickness proportions of MTD facies in logged sections.

et al., 2008; Martín-Merino *et al.*, 2014; Miramontes *et al.*, 2016).

DISCUSSION

MTD geometry and sedimentary facies partitioning

In the *Turbidites* section, it has been shown that, even though geometry and correlation of the turbidite stratigraphy immediately above indicate an overall flat MTD top, there are a few localities where the lower 5 to 15 m of this turbidite sequence is partly (logs S11 and S28; Fig. 4) or completely (log S3; Fig. 4) missing. This observation suggests that when the first post-MTD turbidites were deposited, these localities constituted bathymetric highs with differential elevations of up to *ca* 15 m (undecompacted) and slopes locally greater than *ca* 5° (for example, bathymetric high of log S3 in Fig. 4). The universal presence of the marlstone conglomerate suggests that these bathymetric highs must have formed only after its deposition; given its high-density character (see interpretation in *Marlstone conglomerate* section) the flow depositing the conglomerate is not expected to have been able to run up and deposit on top of topographic highs. Rather, it was probably steered through the relief of the deposit below, burying it under a variably thick and relatively flat-topped deposit. It is thus concluded that soon after deposition, the top of the investigated part of the MTD was essentially flat and that localized bathymetric highs might have formed because of post-depositional lateral and vertical movements of the MTD components driven by gravity and/or by early differential compaction (e.g. Alves, 2010; Kneller *et al.*, 2016).

The MTD top can therefore be used as a datum surface on which to flatten sedimentary logs so as to gain insights into likely geometry of the MTD basal erosion. When flattening sedimentary logs on the MTD top, the notion of a substantially flat deposit top is strengthened by similarly flat geometry of the marker turbidite beds below and above the MTD (Figs 4 and 12). The values of depth of basal erosion calculated at each logged locality (see methods in *Data, methods and terminology* section) are the constraints used to hand-draw erosion depth

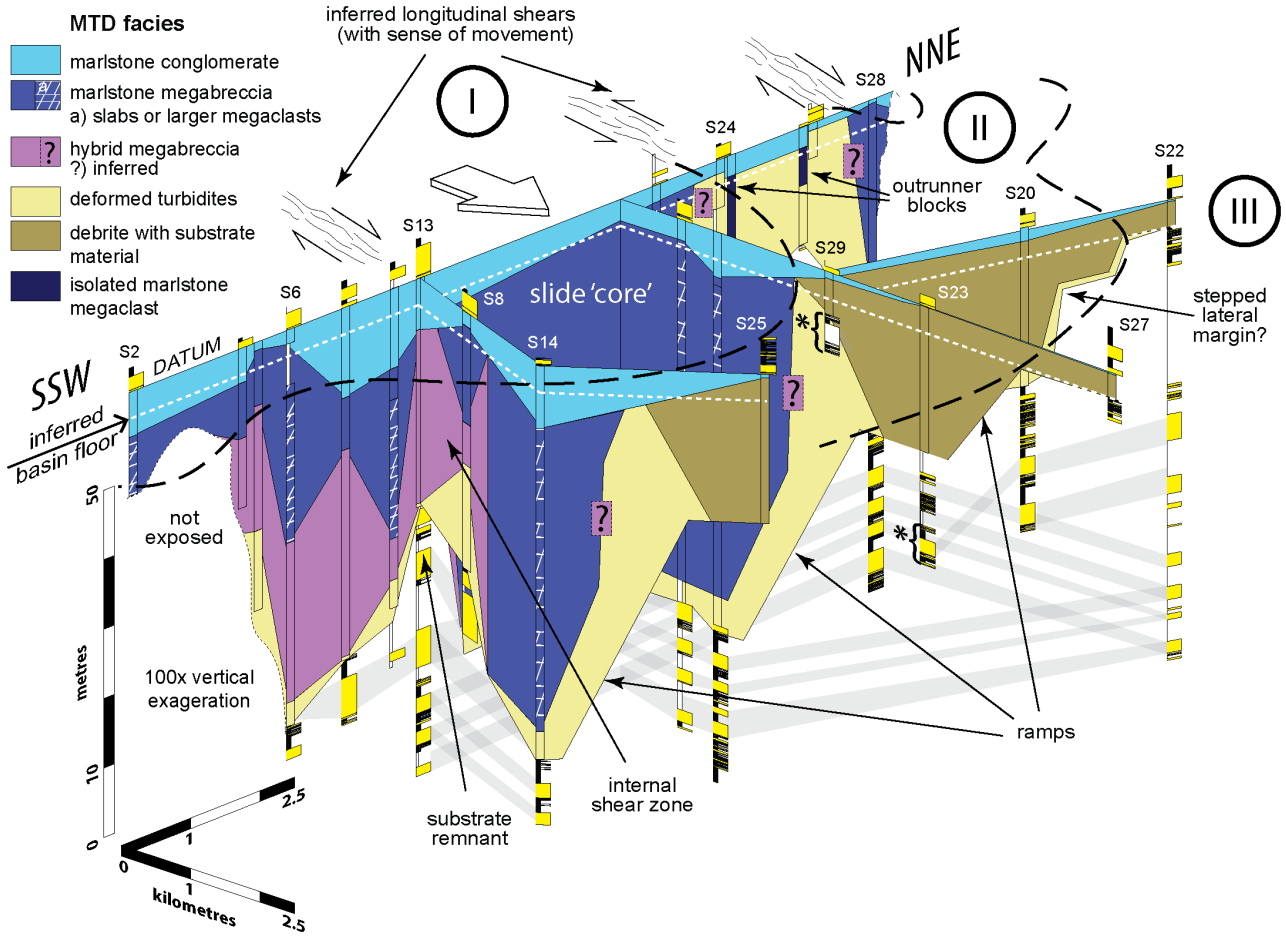

Fig. 12. Fence diagram (see Fig. 11 for location) of the Mt. Olivastro mass transport deposit (MTD) illustrating the spatial relationship between component facies with interpretation provided in the *Spatio-temporal evolution of the mass flow and role of substrate interaction* section. The white arrow indicates transport direction. The dashed black lines indicate the inferred boundaries of the MTD domains introduced in the *MTD geometry and sedimentary facies partitioning* section (identified by roman numerals; I: erosionally confined megabreccia; II: ramp and flat sector; III: distal emergent deposit).

contours, reported in Fig. 11 along with MTD sedimentary facies proportions. Depth contours were drawn smoothly with the intention of highlighting first-order variations over smaller-scale features of the MTD basal erosion surface. The gross geometry of the preserved part of the Mt. Olivastro MTD is one where the depth of basal erosion and deposit thickness decrease towards the east (Fig. 11), suggesting a westerly-sourced parental mass flow.

The area around the Mt. Olivastro summit (logs S10, S11 and S26; Fig. 11) represents a zone of deep erosion, locally in excess of 50 m. This is filled mainly by the marlstone megabreccia, which extends to the south as far as log S14 (to the north of the town of Dolceacqua) and contains several large slabs (Fig. 6). It is important to note that log correlations suggest that the top surface of the marlstone megabreccia appears rugose at a range of scales but generally lies below the inferred pre-MTD basin floor level (i.e. the top of the youngest turbidite event bed below the MTD), implying that the MTD is largely confined within its basal erosion. To the north, the erosion surface shallows, whilst the megabreccia is rapidly replaced by 10 to 20 m of deformed turbidites (for example, logs S24, S19b and S21) with sparse marlstone megaclasts (Figs 8C, 9D and 11). Farther to the north, the megabreccia reappears in logs S28 and S28b (Fig. 11), but it is unclear whether (and how far to the west) this deposit may connect to that of

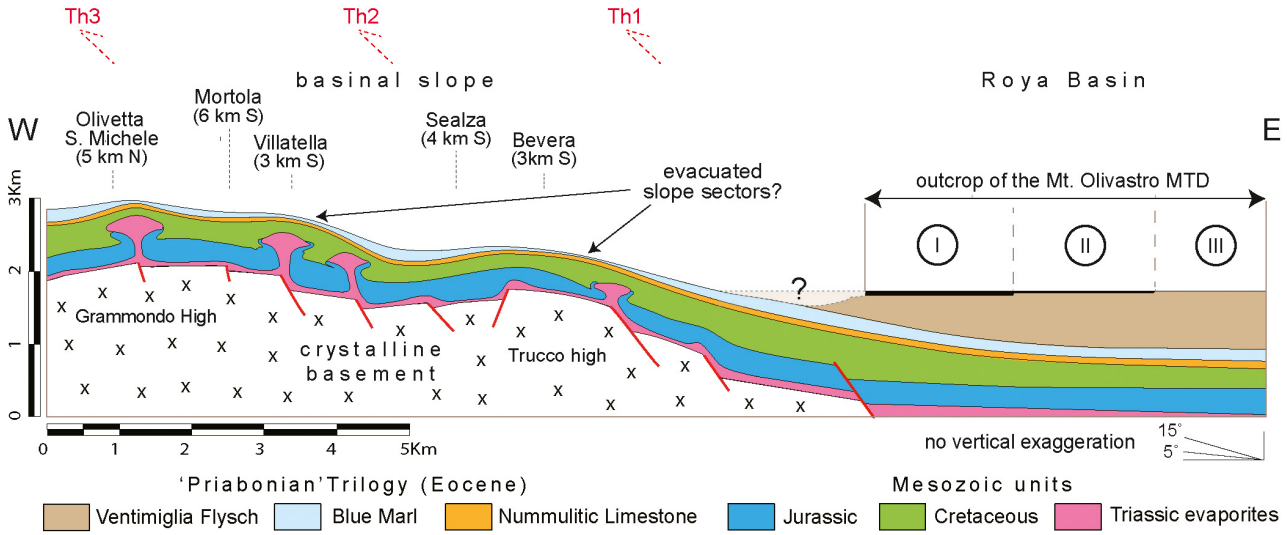

Fig. 13. Idealized representation of the western basinal slope at the time of emplacement of the Mt. Olivastro mass transport deposit (MTD), with location of future thrust faults (see Fig. 2); outcrop localities are projected orthogonally onto the section from both the south (S) and north (N), with distance of projection reported in brackets. The Mt. Olivastro MTD is represented as a black line thinning to the east, with roman numerals identifying the domains detailed in the *Discussion* section (I: erosionally confined megabreccia; II: ramp and flat sector; III: distal emergent deposit). The erosionally confined deposit is only partially preserved today, hampering estimation of its total along-dip length. The thickness of the Blue Marls is based upon the observations of Campredon (1972). Note the association of relatively thin Blue Marls with inferred halokinesis in the Triassic evaporites.

Mt. Olivastro; instead it may represent a subsidiary depositional body emplaced by the same mass wasting event.

The Mt. Olivastro–Dolceacqua erosion also shallows towards the east and the south-west (Fig. 11). To the east, the depth of erosion reduces to *ca* 20 m in sections S20, S23 and S25, and to its minimum observed values in sections S22 and S27, whilst the megabreccia is replaced by the debrite with substrate material. At these latter localities, because the depth of erosion is assumed to be very close to zero, the debrite with substrate material virtually sits upon what was likely the original (undisturbed) basin floor and should thus be called an emergent deposit. To the south-west, the relatively shallow erosion of logs S13 and S8 is instead associated with a thick section of either the hybrid megabreccia type or the deformed turbidites, respectively, which suggests a possible slip boundary separating the Mt. Olivastro–Dolceacqua erosion from that of south-westerly sections (logs S3 to S7). In these south-westerly localities too, the basal erosion is infilled with significant proportions of hybrid megabreccia and, locally, deformed turbidites, and appears to shallow rapidly to the SSE (log S3, Figs 11 and 12).

Lastly, it is noteworthy that the deformed turbidites are the thickest where the basal erosion shallows rapidly (for example, logs S3, S8 and S28; Fig. 11), and can partly lie above the inferred basin floor level (for example, logs S19b, S21 and S24; Figs 4 and 11), suggesting enhanced strain in substrate sediments at MTD margins, locally accompanied with extrusion to the seafloor. In keeping with this hypothesis, the ratio of thickness of marlstone megaclast to thickness of the deformed turbidites in nearby sections (logs S19, S24b and S21b; see Figs 3A and 4 for location) is relatively low (<4) compared to that reported for slide blocks of similar size (Alves & Lourenço, 2010), suggesting that the deformation of substrate sediments in this section of the MTD is not genetically related to sliding of isolated marlstone megaclasts.

To summarize, composition and thickness, in tandem with geometry of the basal erosion can be used to subdivide the preserved part of the Mt. Olivastro MTD into three major domains. From west to east (i.e. proximally to distally), these are an erosionally confined megabreccia (including both the marlstone megabreccia and the compositionally hybrid type; see *Megabreccia* section), a ramp and flat sector, and a distal emergent deposit

that sits upon what was likely the original (undisturbed) basin floor (I, II and III, respectively; Figs 12, 13 and 14F). The significance of these domains will be discussed further in the *Spatio-temporal evolution of the mass flow and role of substrate interaction* section.

Constraints on location, size and character of the failure

The effects of Oligocene contractional tectonics (Apps *et al.*, 2004; Gianmarino *et al.*, 2010; Decarlis *et al.*, 2014; Dallagiovanna *et al.*, 2017) make it difficult to establish the local bathymetry at the time of emplacement of the Mt. Olivastro MTD. However, the westward younging of the age of the onset of the Ventimiglia Flysch deposition (Campredon, 1972; Sztrákos & Fornel, 2003; du Fornel *et al.*, 2004) implies that the turbidites embedding the MTD onlapped onto a broadly east-dipping western slope, which most likely continued to experience hemipelagic deposition up-dip (Fig. 13). Thickness changes in the Blue Marl (Campredon, 1972; Decarlis *et al.*, 2014) suggest that the slope profile was uneven and possibly dynamic. This could have been due to active halokinesis of Triassic evaporites, (documented in a few nearby localities; for example the Grammondo and Trucco highs; Fig. 13) which might have persisted at least until the early Upper Cretaceous (Decarlis *et al.*, 2014). Alternatively, the complexity of the slope profile may reflect syn-depositional activity of hinterland- (eastward-) dipping normal faults (Crampton & Allen, 1995; Tomasso & Sinclair, 2004), or early activation of Alpine thrusts and associated strike slip-faults (Campredon & Giannerini, 1982; Jean *et al.*, 1985; Ravenne *et al.*, 1987; Apps *et al.*, 2004). Both models entail that the western basinal slope adjacent to the Mt. Olivastro MTD was locally over-steepened and hence likely prone to mass wasting.

Locating the source area of the MTD is complicated by the fact that significant portions of the western slope coeval to the Mt. Olivastro MTD have been removed by modern erosion or are hiding in the subsurface, in the hangingwall and the footwall of the Th1 thrust, respectively (Fig. 13). Possible analogues of the Mt. Olivastro MTD source scar might be preserved in a few westerly localities where the Blue Marls show markedly reduced thickness or are absent (for example, Mortola, Villatella and Bevera in Figs 3 and 13) (Franchi, 1926; Campredon, 1972; Dallagiovanna *et al.*, 2017). However, it is unclear whether these sections are the result of mass wasting processes or reflect condensed hemipelagic deposition on top of bathymetric highs; this question requires further investigation.

The lithology and size of the clasts forming the marlstone megabreccia provide constraints on thickness of the failed section and possible setting of the scar. These clasts can unequivocally be recognized as originating from the middle and upper lithofacies of the Blue Marl. Clasts that are more calcareous, suggestive of a deeper source (i.e. the lower lithofacies of the Blue Marl and the Nummulitic Limestone; see *Geological setting* section), are notably missing, and so are lithologies that could indicate involvement of sediments deposited in a shallower environment. This indicates that the basal detachment was relatively shallow, albeit certainly deeper than 30 to 40 m (i.e. the typical stratigraphic thickness of the slabs present in the megabreccia), and that the scar was located in relatively deep water.

The toe ramp of the initial slide could have been located either below the basin floor or higher on the slope. The first scenario implies that the ramp tip was located below the basin floor, at a depth greater or equal to the maximum observed depth of erosion, which seems unlikely as a several tens of metres-thick section of turbidite sediments above, albeit less dense than the failed marlstone material, would have provided sufficient lateral support to the slide so to restrain its lateral translation or at least to dampen significantly its kinetic energy. In the second scenario, shown in Fig. 14A, the slide would have emerged from the scar and translated over some distance along the slope before reaching the basin floor.

The width of the most proximal preserved part of the Mt. Olivastro MTD indicates that the parental failure was moderately wide (at least *ca* 9 km; Fig. 11), suggesting a sector collapse of the slope. The thickness and extent of the preserved megabreccia (Fig. 11) allow the (undecompacted) minimum volume of failed marlstone material to be estimated at *ca* 0.5 km^3. However, geometrical constraints on basin configuration (Fig. 13) suggest that the base of the western slope was located at least a few kilometres to the west of the MTD outcrop, implying that a similar along-dip length of proximal deposit and the associated basal erosion is not preserved today. Therefore, the emergent part of the slide that reached the basin floor had a likely volume of a few to several km^3.

Spatio-temporal evolution of the mass flow and role of substrate interaction

The sheet-like architecture of the turbidites below the Mt. Olivastro MTD (*Turbidites* section) suggests that substrate heterogeneity and seafloor topography are unlikely to have played a significant role on the mass flow pathway and down-dip evolution, for example by steering it or by focusing erosion in areas of more easily remobilized substrate materials (e.g. Ortiz-Karpf *et al.*, 2015, 2017). Therefore, vertical and lateral facies trends of the MTD chiefly reflect the spatio-temporal changes in mass flow rheology, composition and kinetic energy following the interaction with near-seafloor turbidite sediments.

The character of marlstone megabreccia (*Marlstone megabreccia* section), particularly the presence of large megaclasts with internal bedding laying at a low angle with respect to that of the turbidites encasing the MTD, suggests that it originated from fragmentation of a coherent translational slide. Although the degree of lithification may have varied vertically in the Blue Marl (for example, due to burial and changes in clay mineralogy and carbonate content; Bodelle *et al.*, 1971), the widespread brittle deformation observed in the marlstone megabreccia suggests that a significant part of the failed section was lithified.

The slide may have initially translated downslope as one rigid body, starting to fragment upon emerging from the failure scar (and traversing the toe ramp, Fig. 14A) after formation and linkage of a series of high-angle fractures. Focusing of strain along these fractures may have led to progressive disintegration of the slide during its downslope motion, with development of an increasingly higher fraction of relatively finer-grained megabreccia separating progressively smaller megaclasts (Fig. 14B and C). A similar process for formation of megaclast-bearing MTD has been proposed by several authors (Kvalstad *et al.*, 2005; Gee *et al.*, 2006; Callot *et al.*, 2008; Alves & Lourenço, 2010; Jackson, 2011; Martín-Merino *et al.*, 2014; Alves, 2015; de Lima Rodrigues *et al.*, 2020; Nugraha, *et al.*, 2020).

The deep erosion observed in the study area indicates that, upon reaching the basin floor, the slide became coupled to a weak substrate, thus behaving as a no-slip flow (Sobiesiak *et al.*, 2018). Here, owing to the excess density of the dominantly lithified material constituting it, the slide is thought to have penetrated into the less consolidated and less dense substrate sediments down to the maximum depth of erosion (Fig. 14B). From this point onward, the slide might have become sufficiently decoupled from the substrate to keep moving, possibly owing to liquefaction within the near seafloor poorly consolidated sediments (i.e. the deformed turbidites; Fig. 14C). It is unknown whether the maximum observed depth of erosion corresponds to the actual maximum depth of erosion, or if the slide eroded to a deeper level in up-dip locations (see *The marlstone conglomerate: dynamic flow separation or retrogressive failure?* section for further discussion). However, the second scenario seems unlikely, since a deeper erosion up-dip would imply that the slide traversed a stepped basal surface before reaching the outcrop area, which would have favoured greater mixing with the substrate material.

The erosionally confined nature of the marlstone megabreccia (*MTD geometry and sedimentary facies partitioning* section and Fig. 12) indicates that the slide was laterally contained by the substrate in place. Beyond preventing flow expansion and further interaction and mixing with substrate sediments, erosional confinement might have resulted in establishment of a widespread compressional regime within the slide, which may explain the lack of tensile stress indicators (for example, normal faults, chasms and associated neptunian dykes; Bull *et al.*, 2009; Alves, 2015) and injection of liquefied substrate sediments (Callot *et al.*, 2008; Ogata *et al.*, 2012; Sobiesiak *et al.*, 2017; Cardona *et al.*, 2020; de Lima Rodrigues *et al.*, 2020). It can also be argued that, upon impact onto the basin floor and during an early phase of motion, the slide was able to induce resuspension of near seafloor sediments ahead of its leading edge, likely with generation of a linked turbidity current (Fig. 14B).

The erosionally-confined deposit shows an along-strike textural and compositional variability, with the marlstone megabreccia becoming finer-grained and more intensely mixed with substrate material (see *Hybrid megabreccia* section) at the southern, more marginal sector of the MTD (Figs 11 and 12). An increase in mixing with substrate sediments and clast disaggregation at MTD margins has been reported from several case studies (Frey-Martínez *et al.*, 2006; Alves & Cartwright, 2009; Alves, 2010; Joanne *et al.*, 2013; Ortiz-Karpf *et al.*, 2017; Nugraha, *et al.*, 2020) and interpreted to reflect along-strike strain partitioning resulting from increased shear at flow margins. In agreement with this model, it is believed that the hybrid

megabreccia was formed in the outer region of the advancing slide (including its base and leading edge; Fig. 14D) after mixing of relatively fine-grained marlstone material and liquefied turbidite material, and was progressively displaced, accumulating at the margins of the megabreccia (Figs 12 and 14F). The abrupt along-strike juxtaposition of the marlstone megabreccia with large megaclasts and the hybrid megabreccia shown in Fig. 12 may represent the

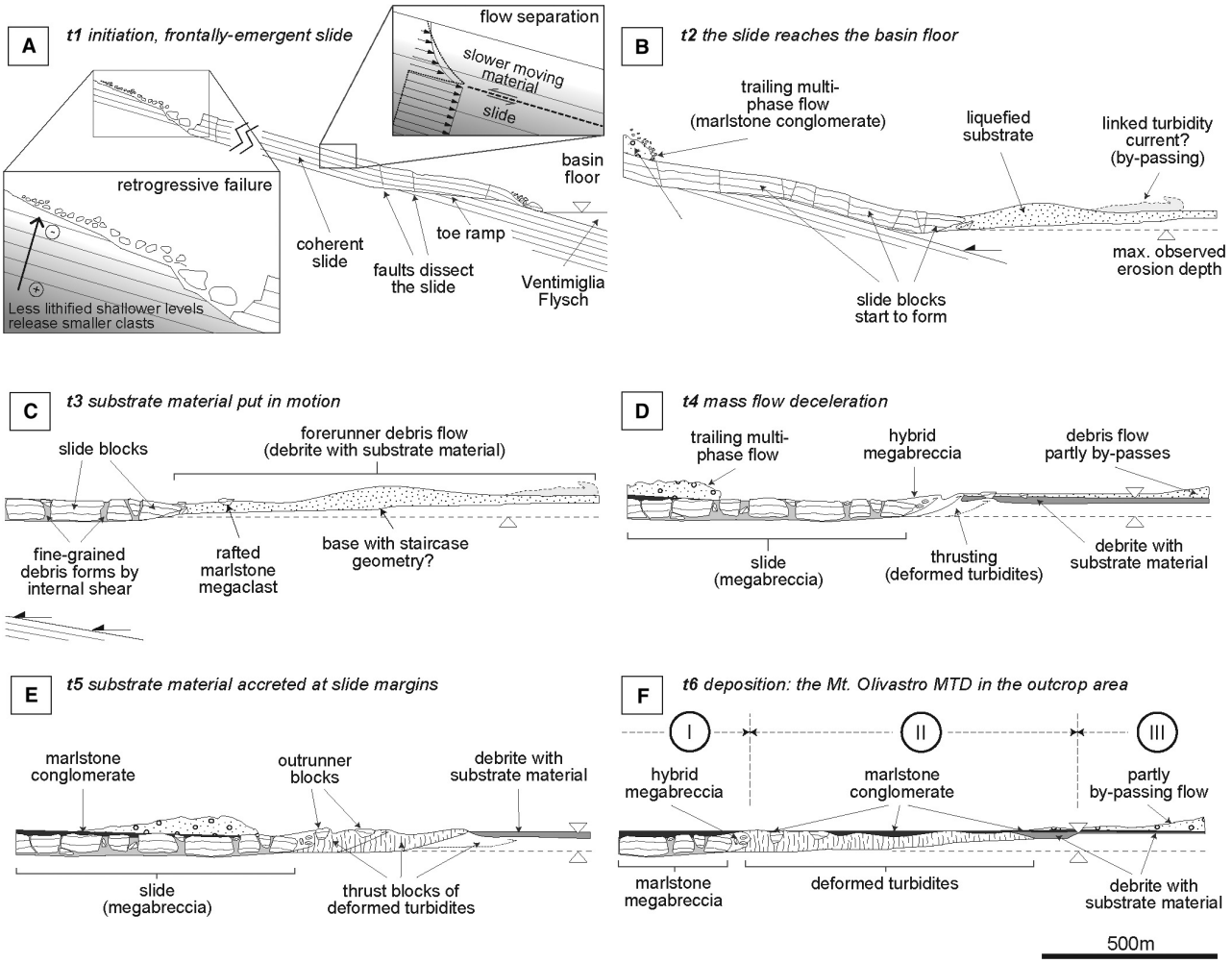

Fig. 14. Inferred transformations in the Mt. Olivastro mass transport deposit (MTD) parental mass flow. (A) The initial slide of Blue Marl emerges from the failure scar and undergoes fragmentation as it traverses the toe ramp. Details highlight the possible retrogressive nature of the failure (lower inset), and the flow separation (upper inset) that likely affected the sliding mass as a result of a vertical gradient of reducing yield strength in the Blue Marl (see *The marlstone conglomerate: dynamic flow separation or retrogressive failure?* section). Both processes may explain the delayed generation of the multiphase trailing flow that will deposit the marlstone conglomerate. (B) The slide intrudes into the substrate sediments inducing their liquefaction and partial resuspension, potentially with generation of a linked turbidity current. (C) Shock wave propagation and associated liquefaction at the leading edge of the slide cause the substrate sediments to move as a (forerunner) debris flow. (D) The slide slows down while the deformed turbidites at its leading edge are entrained by shear detachment and thrusting. The debris-flow deposits the debrite with substrate material and partly bypasses. (E) Accumulation of the deformed turbidites continues as further thrusts form in the substrate, placing them in contact with the debrite with substrate material. In up-dip locations, the trailing multiphase flow is steered through the relief of the megabreccia below, infilling it with the marlstone conglomerate. (F) The slide and the deformation within substrate turbidites come to a halt and are partly by-passed by the trailing multiphase flow, which lays down a distally tapering conglomeratic deposit that compensates for the uneven top of the underlying deposit. Roman numerals in (F) refer to MTD domains (I: erosionally confined megabreccia; II: flat and ramp sector; III distal emergent deposit).

product of a late flow stage protrusion of a less fragmented core region of the slide into its slower moving marginal regions, with the relative slip at boundaries being accommodated by shear zones striking roughly parallel to mass flow direction (*cf.* the longitudinal shears of Bull *et al.*, 2009).

The ramp and flat sector ('II' of Figs 12, 13, 14E and 14F) connects the deep erosion confining the proximal deposit to what is thought to represent the undisturbed pre-MTD basin floor to the west. It is a region surrounding the marlstone megabreccia where the MTD consists of the deformed turbidites facies and, more distally, by the debrite with substrate material (*MTD geometry and sedimentary facies partitioning* section). The lateral contact between deformed turbidites and the debrite with substrate material could not be observed directly, which makes their relationship and relative chronology of emplacement unclear. However, their contrasting sedimentary character (i.e. structure, texture, degree of disaggregation, and mixing with the exotic material) indicates deposition by fundamentally different processes, likely at different stages of MTD emplacement.

The deformed turbidites of the ramp and flat sector show a generally coherent deformation, with intact pieces of stratigraphy that can be correlated with that below the MTD in nearby sections (Figs 4 and 12), and occur at boundaries of the marlstone megabreccia, locally above the inferred basin floor level (*MTD geometry and sedimentary facies partitioning* section). This suggests that they represent substrate material accumulated at mass flow margins after minor lateral and stratigraphic translation. This may have happened when the slide was decelerating and about to come a halt (Fig. 14E and F) after buttressing against the substrate stratigraphy in place. Thus, the deformed turbidites of the ramp and flat sector are best interpreted as part of pop-ups and thrust blocks (Bull *et al.*, 2009) comparable to those forming in the toe region of frontally-emergent MTDs (Joanne *et al.*, 2013; Sobiesiak *et al.*, 2018; Pini *et al.*, 2020).

On the other hand, as discussed further in the *Distal emergent deposit: volume balance and inferred flow run-out* section, volume balance considerations indicate that the debrite with substrate material was deposited from a debris flow that was sufficiently mobile to redistribute distally the turbidite material evacuated from the basal erosion up-dip. This suggests that the debrite was deposited in a stage preceding the development of the deformed turbidites, most likely from a forerunner debris flow developing after liquefaction of substrate sediments ahead of the of the advancing slide (Fig. 14B). Likely analogues for the debrite with substrate material are the distal deposits associated with several submarine slides (Nardin *et al.*, 1979; Gee *et al.*, 2006; Mosher *et al.*, 2010; Brothers *et al.*, 2019), although such deposits are rarely calibrated for lithology (Tripsanas *et al.*, 2008; Sawyer *et al.*, 2009).

Distal emergent deposit: volume balance and inferred flow run-out

The distal deposit sits above what is interpreted to represent the undisturbed pre-MTD basin floor (Fig. 14F). It was observed only in two outcrops (logs S22 and S27; Figs 8A, 11 and 13), where it is represented by a *ca* 5 m thick debrite comprising >90% turbiditic substrate material. Because of tectonic deformation and a limited number of outcrops, the lateral continuity of the deposit is unknown and is unclear whether it passes into a co-genetic turbidite (*Spatio-temporal evolution of the mass flow and role of substrate interaction* section; Fig. 14B). Nevertheless, an attempt can be made to loosely balance the volume of turbidite material displaced from the basal erosion with that in the distal deposit. The basal erosion in the preserved area (Fig. 11) corresponds to a volume of evacuated turbidite material in the order of *ca* 0.5km^3. However, the inferred length (*Constraints on location, size and character of the failure* section) of the proximal erosionally confined part of the MTD (Fig. 14B and C) and the possibility that a deeper erosion existed up-dip of the study area suggest a larger volume, most likely in the order of several km^3. Assuming a 5 m thick tabular geometry, this would imply that the distal deposit should cover an area exceeding a few 100 km^2, suggesting a flow run-out in excess of a few tens of kilometres, which is in the range of those reported in the literature for similar flows (e.g. Mosher *et al.*, 2010; Brothers *et al.*, 2019).

The marlstone conglomerate: dynamic flow separation or retrogressive failure?

In all of the MTDs mapped in the Ventimiglia Flysch (Fig. 3), a marlstone conglomerate (*Marlstone conglomerate* section) caps other mass transport facies, burying their uneven top surfaces, suggesting that it was deposited by a co-genetic flow that lagged behind the slide.

The sedimentary character of the marlstone conglomerate (for example, normal grading and roundness of component clasts) and its

association with the underlying marlstone megabreccia, suggest that most of its clasts originally were early cementation nodules characterizing the less compacted and less cemented upper part of the failed Blue Marl section. Such early cementation nodules, documented elsewhere in a relatively shallow (eogenetic) diagenetic zone in similar argillaceous marlstones (Marsaglia *et al.*, 2017), may have become smaller, less frequent, less interlocked, and less indurated up-section, alongside the decrease in carbonate content characterizing the Blue Marl (Bodelle *et al.*, 1971). Two processes may have acted, either exclusively or in combination, to generate the parent flow that deposited the marlstone conglomerate. The first process is one of flow separation between a faster moving slide, represented by the lithified lower part of the failed section, and a trailing flow involving the poorly lithified and less stiff upper part of the failure (see inset in upper right corner of Fig. 14A). This process, observed in numerous other studies of subaqueous slide dynamics (Mohrig & Marr, 2003; Haflidason *et al.*, 2004; Brothers *et al.*, 2019), might have resulted from vertical variation of yield strength within the failed mass, accompanied with its lithological variability (Bodelle *et al.*, 1971).

Alternatively (or additionally), the trailing flow depositing the conglomerate may have formed because of retrogressive failure, with an increasingly higher fraction of shallow, less cemented sediments involved as the failure plane propagated and shallowed up-slope (see inset in lower left corner Fig. 14A). A similar process has been proposed by Tripsanas *et al.* (2008) to explain vertical facies associations in MTDs from the Gulf of Mexico and offshore Canada. In both of these models, the hypothesized upward decrease in the degree of early cementation within the poorly lithified upper part of the failed section may have caused additional flow separation in the trailing flow, with development of the debris flow and the high-density turbulent flow invoked to explain the vertical organization of the conglomerate (*Marlstone conglomerate* section).

Regardless of the dominant process that generated the conglomerate parental flow, the clast size distribution (including the normal grading) might also reflect a flow-related mechanical degradation process (see the experimental study of Caballero *et al.*, 2014), which, for example, may have contributed to the breakup of cemented nodules.

Likely controls on development of erosional confinement and implications on along-flow deposit heterogeneity

Although a mounded morphology in unpreserved proximal sections cannot be excluded, in the study area the up to *ca* 60 m thick Mt. Olivastro MTD is largely confined within its basal erosion and has a relatively flat top elevated no more than a few metres above the level of the inferred (pre-MTD) basin floor (Figs 12 and 14D). Below the marlstone conglomerate, the top of the megabreccia is highly irregular and lies generally at or below the inferred basin floor, signifying that, in the study area, the incoming slide was effectively fully confined by the substrate in place.

The erosionally confined nature of the Mt. Olivastro MTD may have different explanations. Assuming that the initial slide became frontally-emergent on the slope, via a toe ramp (the scenario shown in Fig. 14A), the observed confinement might have resulted from the slide reaching the study area with just enough kinetic energy to erode into the substrate as deep as its thickness. This option cannot be excluded, but it obviously appears quite fortuitous. Alternatively, the depth of the observed erosional confinement corresponds to a shear strength boundary in the substrate that was deeper than the thickness of the incoming slide.

The degree of erosional confinement (i.e. the ratio of basal erosion depth to deposit top elevation) of the Mt. Oivastro MTD is notably higher than that documented elsewhere, with a depth of erosion one order of magnitude larger than the deposit top elevation. In fact, disregarding outcrop examples, where tying MTD base and top to the contemporaneous seafloor is generally difficult (e.g. Callot *et al.*, 2008; Armitage *et al.*, 2009; Ogata *et al.*, 2014), published subsurface examples of frontally-emergent blocky MTDs (Haflidason *et al.*, 2004; Gee *et al.*, 2006; Joanne *et al.*, 2013; Alves, 2015; Kneller *et al.*, 2016; Brothers *et al.*, 2019; Nwoko *et al.*, 2020) show mounded tops with elevations within the same order of magnitude as depth of basal erosion; this may be because most seismically imaged MTDs are significantly thicker than the depth at which the substrate shear strength likely exceeds the shear stress from the overriding flow. It is possible, therefore, that thicker flows passing over firmer substrates cause shallower erosion and produce mounded MTDs, whereas thinner flows and weaker substrates cause erosional confinement

and produce quasi-flat topped MTDs. The former may be characterized by relatively minor along-dip facies and compositional variability, whereas the latter may exhibit rapid down-flow transitions from (erosionally confined) exotic slide materials to distal emergent deposits made dominantly of substrate material, as seen in the Mt. Olivastro MTD. Thus, in erosionally confined scenarios, the kinetic energy of the incoming slide may be transferred to the substrate material evacuated from the basal erosion, so that the mass flow propagates as a single dynamic event while the original constituent material is largely replaced by material entrained from the substrate. This topic requires further study but has important implications for the composition of frontally-emergent MTDs.

CONCLUSIONS

The up to *ca* 60 m thick Mt. Olivastro mass-transport deposit (MTD) constitutes part of the Ventimiglia Flysch of north-west Italy, the turbidite infill of the innermost and oldest depocentre of the Alpine Tertiary foreland basin. It is a frontally-emergent blocky MTD comprised of slope-derived marlstones, representing the original slide, and turbidite material, entrained after erosion of poorly consolidated substrate sediments. Gross deposit geometry and the character of the marlstone clasts indicate that the initial slide originated from a sector collapse of the western basinal slope that involved a several tens of metres-thick section of variably consolidated marlstones. Thickness and facies changes, correlated over an outcrop area of *ca* 40 km^2, provide the following insights into MTD architecture and the downstream transformation of its parental mass flow as it transitioned from an erosionally confined to an emergent state:

- The preserved part of the Mt. Olivastro MTD represents a relatively flat-topped morphotype with a basal erosion up to 55 m deep and a top elevated no more than a few metres above the (pre-MTD) basin floor.
- Correlations within the hosting turbidite stratigraphy highlight an erosionally confined proximal deposit and a distal emergent deposit, connected via a ramp and flat sector.
- The erosionally confined deposit comprises a marlstone megabreccia with megaclasts up to *ca* 1 km that originated after fragmentation of the initial slide overlying a thin basal shear layer of deformed turbidites.
- Sitting upon the undisturbed basin floor, the distal emergent deposit is a debrite formed of substrate material and with rare marlstone clasts up to megaclasts in size; it was laid down by a forerunning debris flow that formed after liquefaction of substrate sediments ahead of the advancing slide.
- The ramp and flat sector is composed of deformed turbidites with sparse outrunner marlstone blocks and, more distally, by the debrite with substrate material. Entrained via shear detachment, the deformed turbidites became part of the slide shortly before it came to a halt.
- The MTD terminates upward into a few to several metres-thick normally graded marlstone conglomerate with a thin marly mudstone cap, which compensates for the uneven top of the underlying deposit. This conglomerate was deposited by a late-stage flow that transported the poorly lithified part of the failed section, with the relatively rounded clasts resulting from flow-related mechanical degradation of early-cementation nodules.
- Volume balancing arguments suggest that the distal emergent deposit may have extended tens of kilometres downstream, highlighting how entrainment of substrate material and linked flow transformation can significantly augment run-out.
- It is suggested that frontally-emergent slides translating over firmer substrates may be associated with shallower erosion and less along-dip facies and compositional variability, whereas weak substrates may result in greater erosion, rapid facies changes, and possibly in a longer run-out of the linked flow charged with substrate material.

ACKNOWLEDGEMENTS

Alfredo Cerliani and Michele Azzarone are thanked for helping with data collection during an early stage of the work. Tiago Alves, Euan Soutter, Matheus Silveira Sobiesiak and an anonymous reviewer are warmly thanked for their insightful reviews. The work was part-funded by the Turbidites Research Group, who thank sponsors AkerBP, CNOOC, ConocoPhillips, Murphy, OMV and Oxy. Open Access

Funding provided by Universita degli Studi di Milano within the CRUI-CARE Agreement.

DATA AVAILABILITY STATEMENT

Research data are not shared.

REFERENCE

Alves, T.M. (2010) 3D Seismic examples of differential compaction in mass-transport deposits and their effect on post-failure strata. *Mar. Geol.*, **271**(3–4), 212–224.

Alves, T.M. (2015) Submarine slide blocks and associated soft-sediment deformation in deep-water basins: A review. *Mar. Pet. Geol.*, **67**, 262–285.

Alves, T.M. and **Cartwright, J.A.** (2009) Volume balance of a submarine landslide in the Espírito Santo Basin, offshore Brazil: quantifying seafloor erosion, sediment accumulation and depletion. *Earth. Planet. Sc. Lett*, **288**(3–4), 572–580.

Alves, T.M. and **Lourenço, S.D.** (2010) Geomorphologic features related to gravitational collapse: Submarine landsliding to lateral spreading on a Late Miocene-Quaternary slope (SE Crete, eastern Mediterranean). *Geomorphology*, **123**(1–2), 13–33.

Amerman, R., **Nelson, E.P.**, **Gardner, M.H.** and **Trudgill, B.** (2011) Submarine mass transport deposits of the Permian Cutoff Formation, West Texas, USA: internal architecture and controls on overlying reservoir sand deposition. Mass-Transport Deposits in Deepwater Settings. *SEPM Spec. Publ.*, **96**, 235–267.

Apps, G.M. (1987) *The Evolution of the Grès d'Annot Basin, SW Alps*. Doctoral Dissertation. University of Liverpool, Liverpool.

Apps, G., **Peel, F.** and **Elliott, T.** (2004) The structural setting and palaeogeographical evolution of the Grès d'Annot basin. *Geol. Soc. Spec. Publ.*, **221**(1), 65–96.

Armitage, D.A., **Romans, B.W.**, **Covault, J.A.** and **Graham, S.A.** (2009) The influence of mass-transport-deposit surface topography on the evolution of turbidite architecture: The Sierra Contreras, Tres Pasos Formation (Cretaceous), southern Chile. *J. Sediment. Res.*, **79**(5), 287–301.

Biancardi, C.A., **Alves, T.M.** and **Martins-Ferreira, M.A.C.** (2020) Unpredictable geometry and depositional stacking patterns of mass-transport complexes in salt minibasins. *Mar. Pet. Geol.*, **120**, 104522. https://doi.org/10.1016/j.marpetgeo.2020.104522

Blair, T.C. and **McPherson, J.G.** (1999) Grain-size and textural classification of coarse sedimentary particles. *J. Sed. Res.*, **69**(1), 6–19.

Bodelle, J., **Campredon, R.**, **Chateauneuf, J.** and **Lezaud, L.** (1971) Le Nummulitique des Scaffarels (France-Basses-Alpes). Utilisation simultanée de plusieurs méthodes d'études stratigraphiques et géochimiques. *Ann. Inst. Géol. Publ Hung*, **54**, 45–63.

Boussac, J. (1912) Ètudes stratigraphique sur le Nummulitique alpin. Mém. Serv. Carte Géol. Fr. 662, 20 pl., Paris.

Brothers, D.S., **Maier, K.L.**, **Kluesner, J.W.**, **Conrad, J.E.** and **Chaytor, J.D.** (2019) The Santa Cruz Basin submarine landslide complex, southern California: Repeated failure of uplifted basin sediment. *J. Sediment. Res.*, **17**(1), 117–134.

Bryn, P., **Berg, K.**, **Forsberg, C.F.**, **Solheim, A.** and **Kvalstad, T.J.** (2005) Explaining the Storegga slide. *Mar. Pet. Geol.*, **22**(1–2), 11–19.

Bull, S., **Cartwright, J.** and **Huuse, M.** (2009) A review of kinematic indicators from mass-transport complexes using 3D seismic data. *Mar. Pet. Geol.*, **26**(7), 1132–1151.

Caballero, L., **Sarocchi, D.**, **Soto, E.** and **Borselli, L.** (2014) Rheological changes induced by clast fragmentation in debris flows. *J. Geophys. Res.*, **119**(9), 1800–1817.

Callot, P., **Sempere, T.**, **Odonne, F.** and **Robert, E.** (2008) Giant submarine collapse of a carbonate platform at the Turonian-Coniacian transition: the Ayabacas Formation, southern Peru. *Bas. Res.*, **20**(3), 333–357.

Camerlenghi, A., **Urgeles, R.** and **Fantoni, L.** (2010) A Database on Submarine Landslides of the Mediterranean Sea. In: *Submarine Mass Movements and Their Consequences* (Eds Mosher, D.C., Shipp, R.C., Moscardelli, L., Chaytor, J.D., Baxter, C.D.P., Lee, H.J. and Urgeles, R.), pp. 503–513. Springer, Dordrecht.

Campredon, R. (1972) *Les formations paléogènes des Alpes maritimes franco-italiennes*. Doctoral Dissertation. Université de Nice-Sophia Antipolis, Faculté des sciences, Nice.

Campredon, R. and **Giannerini, G.** (1982) Le synclinal de Saint-Antonin (arc de Castellane, chaînes subalpines méridionales) Un exemple de bassin soumis à une déformation compressive permanente depuis l'Eocène supérieur. *Géol. Alp.*, **58**, 15–20.

Cardona, S., **Wood, L.J.**, **Dugan, B.**, **Jobe, Z.**, **Strachan, L.J.** and **Baas, J.** (2020) Characterization of the Rapanui mass-transport deposit and the basal shear zone: Mount Messenger Formation, Taranaki Basin, New Zealand. *Sedimentology*, **67**(4), 2111–2148.

Charollois, J., **Hochuli, P.A.**, **Oertli, H.J.**, **Perch-Nielsen, K.**, **Toumarkine, M.**, **Rögl, F.** and **Pairis, J.L.** (1980) Les Marnes à Foraminifères et les Schistes à Meletta des chaînes subalpines septentrionales (Haute-Savoie, France). *Eclogae Geol. Helv.*, **73**(1), 6–69.

Crampton, S.L. and **Allen, P.A.** (1995) Recognition of forebulge unconformities associated with early stage foreland basin development: example from the North Alpine Foreland Basin. *Am. Ass. Pet. Geol. Bull*, **79**(10), 1495–1514.

Dallagiovanna, G., **Fanucci, F.**, **Pellegrini, L.**, **Seno, S.**, **Bonini, L.**, **Decarlis, A.**, **Maino, M.**, **Morelli, D.** and **Toscani, G.** (2017) *Note Illustrative della Carta Geologica D'Italia alla scala 1:50000, Foglio 257 Dolceacqua e Foglio 270 Ventimiglia*. ISPRA, Firenze, 103 pp.

Dardeau, G. and **De Graciansky, P.C.** (1990) Halocinèse et rifting téthysien dans les Alpes-Maritimes (France). *Bull. Cent. Rech. Explor. Prod. Elf Aquitaine*, **14**(2), 443–464.

De Blasio, F.V., **Engvik, L.E.** and **Elverhøi, A.** (2006) Sliding of outrunner blocks from submarine landslides. *Geophys. Res. Lett.*, **33**, L06614. https://doi.org/10.1029/2005GL025165

De Graciansky, P.C., **Roberts, D.G.** and **Tricart, P.** (2011) *The Western Alps, from Rift to Passive Margin to Orogenic Belt: An Integrated Geoscience Overview*, Vol. **14**. Elsevier, Amsterdam. 432 pp.

Decarlis, A., **Dallagiovanna, G.**, **Lualdi, A.**, **Maino, M.** and **Seno, S.** (2013) Stratigraphic evolution in the Ligurian alps between Variscan heritages and the Alpine Tethys opening: A review. *Earth-Sci. Rev.*, **125**, 43–68.

Decarlis, A., **Maino, M.**, **Dallagiovanna, G.**, **Lualdi, A.**, **Masini, E.**, **Seno, S.** and **Toscani, G.** (2014) Salt tectonics in the SW Alps (Italy–France): From rifting to the inversion of the European continental margin in a context of oblique convergence. *Tectonophysics*, **636**, 293–314.

Du Fornel, E., **Joseph, P.**, **Desaubliaux, G.**, **Eschard, R.**, **Guillocheau, F.**, **Lerat, O.**, **Muller, C.**, **Ravenne, C.** and **Sztrakos, K.** (2004) The southern Grès d'Annot outcrops (French Alps): an attempt at regional correlation. *Geol. Soc. Spec. Publ*, **221**(1), 137–160.

Elliott, T., **Apps, G.**, **Davies, H.**, **Evans, M.**, **Ghibaudo, G.** and **Graham, R.H.** (1985) A structural and sedimentological traverse through the Tertiary foreland basin of the external Alps of south-east France. In: *International Symposium on Foreland Basins*. Excursion guide book, International Association of Sedimentologists, Fribourg, pp. 73.

Fallgatter, C., **Kneller, B.**, **Paim, P.S.** and **Milana, J.P.** (2017) Transformation, partitioning and flow–deposit interactions during the run-out of megaflows. *Sedimentology*, **64**(2), 359–387.

Ford, M., **Lickorish, W.H.** and **Kusznir, N.J.** (1999) Tertiary foreland sedimentation in the Southern Subalpine Chains, SE France: a geodynamic appraisal. *Basin Res*, **11**(4), 315–336.

Franchi, S. (1926) *Carta geologica del Regno al 1: 100000-foglio 102*. R. Uff. Geologico, San Remo, Roma.

Frey-Martínez, J., **Cartwright, J.** and **James, D.** (2006) Frontally confined versus frontally emergent submarine landslides: A 3D seismic characterisation. *Mar. Petrol. Geol*, **23**(5), 585–604.

Gamboa, D. and **Alves, T.M.** (2015) Three-dimensional fault meshes and multi-layer shear in mass-transport blocks: implications for fluid flow on continental margins. *Tectonophysics*, **647**, 21–32.

Gee, M.J.R., **Gawthorpe, R.L.** and **Friedmann, S.J.** (2006) Triggering and evolution of a giant landslide, offshore Angola revealed by 3D seismic stratigraphy and geomorphology. *J. Sed. Res*, **76**, 9–19.

Georgiopoulou, A., **Masson, D.G.**, **Wynn, R.B.** and **Krastel, S.** (2010) Sahara Slide: Age, initiation, and processes of a giant submarine slide. *Geochem. Geophy. Geosy*, **11**(7).

Gianmarino, S., **Fanucci, F.**, **Orezzi, S.**, **Rosti, D.** and **Morelli, D.** (2010) *Note Illustrative della Carta Geologica D'Italia alla scala 1:50.000, foglio 258–271 San Remo*. ISPRA, Firenze, 130 pp.

Haflidason, H., **Sejrup, H.P.**, **Nygård, A.**, **Mienert, J.**, **Bryn, P.**, **Lien, R.**, **Forsberg, C.F.**, **Berg, K.** and **Masson, D.** (2004) The Storegga Slide: architecture, geometry and slide development. *Mar. Geol.*, **213**(1–4), 201–234.

Ikari, M.J. and **Kopf, A.J.** (2015) The role of cohesion and overconsolidation in submarine slope failure. *Mar. Geol.*, **369**, 153–161.

Jackson, C.A.L. (2011) Three-dimensional seismic analysis of megaclast deformation within a mass transport deposit; implications for debris flow kinematics. *Geology*, **39**(3), 203–206.

Jean, S., **Kerckhove, C.**, **Perriaux, J.** and **Ravenne, C.** (1985) Un modèle paléogène de bassin a turbidites: les Grès d'Annot du massif de l'Argentera-Mercantour. *Géol. Alp.*, **61**, 115–143.

Joanne, C., **Lamarche, G.** and **Collot, J.Y.** (2013) Dynamics of giant mass transport in deep submarine environments: the Matakaoa Debris Flow, New Zealand. *Basin Res*, **25**(4), 471–488.

Joseph, P. and **Lomas, S.A.** (2004) Deep-water sedimentation in the Alpine Foreland Basin of SE France: New perspectives on the Grès d'Annot and related systems - an introduction. In: *Deep-Water Sedimentation in the Alpine Basin of SE France: New Perspectives on the Grès d'Annot and Related Systems* (Eds Joseph, P. and Lomas, S.A.). *Geol. Soc. Spec. Publ.*, **221**, 1–16.

Kneller, B., **Dykstra, M.**, **Fairweather, L.** and **Milana, J.P.** (2016) Mass-transport and slope accommodation: implications for turbidite sandstone reservoirs. *Am. Assoc. Pet. Geol. Bull*, **100**(2), 213–235.

Kneller, B. and **McCaffrey, W.** (1999) Depositional effects of flow nonuniformity and stratification within turbidity currents approaching a bounding slope; deflection, reflection, and facies variation. *J. Sed. Res.*, **69**(5), 980–991.

Kvalstad, T.J., **Andresen, L.**, **Forsberg, C.F.**, **Berg, K.**, **Bryn, P.** and **Wangen, M.** (2005) The Storegga slide: evaluation of triggering sources and slide mechanics. In *Ormen Lange–an Integrated Study for Safe Field Development in the Storegga Submarine Area*, **22**, pp. 245–256. Elsevier.

de Lima Rodrigues, M.C.N., **Trzaskos, B.**, **Alsop, G.I.** and **Vesely, F.F.** (2020) Making a homogenite: An outcrop perspective into the evolution of deformation within mass-transport deposits. *Mar. Pet. Geol*, **112**, 104033.

Marsaglia, K.M., **Browne, G.H.**, **George, S.C.**, **Kemp, D.B.**, **Jaeger, J.M.**, **Carson, D.** and **Richaud, M.** (2017) The transformation of sediment into rock: insights from IODP Site U1352, Canterbury Basin, New Zealand. *J. Sediment. Res.*, **87**(3), 272–287.

Martín-Merino, G., **Fernández, L.P.**, **Colmenero, J.R.** and **Bahamonde, J.R.** (2014) Mass-transport deposits in a Variscan wedge-top foreland basin (Pisuerga area, Cantabrian Zone, NW Spain). *Mar. Geol*, **356**, 71–87.

Martinsen, O.J. (1994) Mass movements. In: *The Geological Deformation of Sediments* (Ed. Maltman, A.), pp. 127–165. Chapman & Hall, London.

McAdoo, B.G., **Pratson, L.F.** and **Orange, D.L.** (2000) Submarine landslide geomorphology, US continentalslope. *Mar. Geol.*, **169**, 103–136.

Miramontes, E., **Cattaneo, A.**, **Jouet, G.** and **Garziglia, S.** (2016) Implications of sediment dynamics in mass transport along the Pianosa Ridge (Northern Tyrrhenian Sea). In: *Submarine Mass Movements and Their Consequences* (Eds Mosher, D.C., Shipp, R.C., Moscardelli, L., Chaytor, J.D., Baxter, C.D.P., Lee, H.J. and Urgeles, R.), pp. 301–309. Springer, Dordrecht.

Moernaut, J., **Wiemer, G.**, **Reusch, A.**, **Stark, N.**, **De Batist, M.**, **Urrutia, R.**, **de Guevara, B.L.**, **Kopf, A.** and **Strasser, M.** (2017) The influence of overpressure and focused fluid flow on subaquatic slope stability in a formerly glaciated basin: Lake Villarrica (South-Central Chile). *Mar. Geol.*, **383**, 35–54.

Mohrig, D. and **Marr, J.G.** (2003) Constraining the efficiency of turbidity current generation from submarine debris flows and slides using laboratory experiments. *Mar. Pet. Geol.*, **20**(6–8), 883–899.

Moscardelli, L. and **Wood, L.** (2008) New classification system for mass transport complexes in offshore Trinidad. *Basin Res.*, **20**(1), 73–98.

Moscardelli, L. and **Wood, L.** (2015) Morphometry of mass-transport deposits as a predictive tool. *Geol. Soc. Am. Bull.*, **B31221**, 1.

Mosher, D.C., **Xu, Z.** and **Shimeld, J.** (2010) The Pliocene Shelburne mass-movement and consequent tsunami, western Scotian Slope. In: *Submarine Mass Movements and Their Consequences* (Eds Mosher, D.C., Shipp, R.C.,

Moscardelli, L., Chaytor, J.D., Baxter, C.D.P., Lee, H.J. and Urgeles, R.), pp. 765–775. Springer, Dordrecht.

Mougin, C. (1978) *Contribution à l'étude des sédiments tertiaires de la partie orientale du synclinal d'Annot (Alpes de Haute Provence). Stratigraphie, géochimie, micropaleontology*. Unpublished Ph.D. Thesis. Université scientifique et médicale de Grenoble, Grenoble.

Mulder, T. and **Alexander, J.** (2001) The physical character of subaqueous sedimentary density flows and their deposits. *Sedimentology*, **48**(2), 269–299.

Mulder, T. and **Etienne, S.** (2014) Discovery of an outcropping Mass Transport Deposit (MTD) in the Palaeogene subalpine synclines of southeastern France: Implications on flexural sub-basin deformation. *Comptes Rendus Géosci.*, **346**(1–2), 37–44.

Nardin, T.R., **Edwards, B.D.** and **Gorsline, D.S.** (1979) Santa Cruz Basin, California Borderland: Dominance of slope processes in basin sedimentation. In *Geology of Continental Slopes* (Eds Doyle, L.J. and Pilkey, O.H.), *SEPM Spec. Publ*, **27**, 209–221.

Nelson, C.H., **Escutia, C.**, **Damuth, J.E.** and **Twichell, D.C.** (2011) Interplay of mass-transport and turbidite-system deposits in different active tectonic and passive continental margin settings: external and local controlling factors. *Sediment. Geol.*, **96**, 39–66.

Nemec, W. (1990) Aspects of sediment movement on steep delta slopes. In: *Coarse- Grained Deltas* (Ed. Prior, D.B.), *International Association of Sedimentologists Spec. Publ.*, **27**, 29–73.

Nugraha, H.D., **Jackson, C.A.L.**, **Johnson, H.D.** and **Hodgson, D.M.** (2020) Lateral variability in strain along the toewall of a mass transport deposit: a case study from the Makassar Strait, offshore Indonesia. *J. Geol. Soc.*, **177**(6), 1261–1279.

Nwoko, J., **Kane, I.** and **Huuse, M.** (2020) Mass transport deposit (MTD) relief as a control on post-MTD sedimentation: Insights from the Taranaki Basin, offshore New Zealand. *Mar. Pet. Geol.*, **120**, 104489.

Nygard, A., **Sejrup, H.P.**, **Haflidason, H.** and **King, E.L.** (2002) Geometry and genesis of glacigenic debris flows on the North Sea Fan; TOBI imagery and deep-tow boomer evidence. *Mar. Geol.*, **188**(1–2), 15–33.

Ogata, K., **Mountjoy, J.J.**, **Pini, G.A.**, **Festa, A.** and **Tinterri, R.** (2014) Shear zone liquefaction in mass transport deposit emplacement: a multi-scale integration of seismic reflection and outcrop data. *Mar. Geol.*, **356**, 50–64.

Ogata, K., **Mutti, E.**, **Pini, G.A.** and **Tinterri, R.** (2012) Mass transport-related stratal disruption within sedimentary mélanges: examples from the northern Apennines (Italy) and south-central Pyrenees (Spain). *Tectonophysics*, **568**, 85–199.

Ortiz-Karpf, A., **Hodgson, D.M.** and **McCaffrey, W.D.** (2015) The role of mass-transport complexes in controlling channel avulsion and the subsequent sediment dispersal patterns on an active margin: the Magdalena Fan, offshore Colombia. *Mar. Pet. Geol.*, **64**, 58–75.

Ortiz-Karpf, A., **Hodgson, D.M.**, **Jackson, C.A.L.** and **McCaffrey, W.D.** (2017) Influence of seabed morphology and substrate composition on mass-transport flow processes and pathways: insights from the Magdalena Fan, offshore Colombia. *J. Sediment. Res.*, **87**(3), 189–209.

Patacci, M. (2016) A high-precision Jacob's staff with improved spatial accuracy and laser sighting capability. *Sed. Geol.*, **335**, 66–69.

Payros, A., **Pujalte, V.** and **Orue-Etxebarria, X.** (1999) The South Pyrenean Eocene carbonate megabreccias revisited: new interpretation based on evidence from the Pamplona Basin. *Sed. Geol.*, **125**(3–4), 165–194.

Payros, A. and **Pujalte, V.** (2019) Eocene mass-transport deposits in the basque basin (Western Pyrenees, Spain) insights into mass-flow transformation and bulldozing processes. In: *Submarine Landslides: Subaqueous Mass Transport Deposits from Outcrops to Seismic Profiles* (Eds Ogata, K., Festa, A. and Pini, G.A.), *American Geophysical Union*, Geophysical Monograph. **246**, pp. 155–170. John Wiley & Sons Inc, Hoboken, NJ.

Pickering, K.T. & **Hiscott, R.N.** (1985) Contained (reflected) turbidity currents from the Middle Ordovician Cloridorme Formation, Quebec, Canada: An alternative to the antidune hypothesis. *Sedimentology*, **32**(3), 373–394.

Pini, G.A., **Lucente, C.C.**, **Venturi, S.** and **Ogata, K.** (2020) Mass-Transport Complexes of the Marnoso-arenacea Foredeep Turbidite System (Northern Apennines, Italy) A Reappraisal After Twenty-Years. In: *Submarine Landslides: Subaqueous Mass Transport Deposits from Outcrops to Seismic Profiles* (Eds Ogata, K., Festa, A. and Pini, G.A.), *American Geophysical Union*, Geophysical Monograph. **246**, 117–137. John Wiley & Sons Inc, Hoboken, NJ.

Posamentier, H.W. and **Martinsen, O.J.** (2011) The character and genesis of submarine mass transport deposits: insights from outcrop and 3d seismic data. In: *Mass-Transport Deposits in Deepwater Settings* (Eds Shipp, R.C., Weimer, P. and Posamentier, H.W.), *SEPM Spec. Publ.*, **96**, 7–38. https://doi.org/10.2110/sepmsp.096.007

Principaud, M., **Mulder, T.**, **Gillet, H.** and **Borgomano, J.** (2015) Large-scale carbonate submarine mass-wasting along the northwestern slope of the Great Bahama Bank (Bahamas): Morphology, architecture, and mechanisms. *Sed. Geol.*, **317**, 27–42.

Puga-Bernabeu, A., **Beaman, R.J.**, **Webster, J.M.**, **Thomas, A.L.** and **Jacobsen, G.** (2017) Gloria Knolls Slide: A prominent submarine landslide complex on the Great Barrier Reef margin of north-eastern Australia. *Mar. Geol.*, **385**, 68–83.

Ravenne, C., **Riche, P.**, **Tremolieres, P.** and **Vially, R.** (1987) Sédimentation et tectonique dans le bassin marin Eocène supérieur-Oligocène des Alpes du Sud. *Revue De L'institut Français Du Pétrole*, **42**(5), 529–553.

Sawyer, D.E., **Flemings, P.B.**, **Dugan, B.** and **Germaine, J.T.** (2009) Retrogressive failures recorded in mass transport deposits in the Ursa Basin, Northern Gulf of Mexico. *J. Geophys. Res. Solid Earth*, **114**(B10).

Sawyer, D.E., **Flemings, P.B.**, **Buttles, J.** and **Mohrig, D.** (2012) Mudflow transport behavior and deposit morphology: Role of shear stress to yield strength ratio in subaqueous experiments. *Mar. Geol.*, **307**, 28–39.

Shanmugam, G. and **Wang, Y.** (2015) The landslide problem. *J. of Palaeogeogr.*, **4**(2), 109–166.

Sinclair, H.D. (1997) Tectono-stratigraphic model for underfilled peripheral foreland basins: an Alpine perspective. *Geol. Soc. Am. Bull*, **109**, 324–346.

Sobiesiak, M.S., **Alsop, G.I.**, **Kneller, B.** and **Milana, J.P.** (2017) Sub-seismic scale folding and thrusting within an exposed mass transport deposit: a case study from NW Argentina. *J. Struct. Geol*, **96**, 176–191.

Sobiesiak, M.S., **Buso, V.V.**, **Kneller, B.**, **Alsop, G.I.** and **Milana, J.P.** (2019) Block Generation, Deformation, and Interaction of Mass-Transport Deposits With the Seafloor:

An Outcrop-Based Study of the Carboniferous Paganzo Basin (Cerro Bola, NW Argentina). In: *Submarine Landslides: Subaqueous Mass Transport Deposits from Outcrops to Seismic Profiles* (Eds Ogata, K., Festa, A. and Pini, A.G.), **246**, pp. 91–104. Geophysical Monograph. John Wiley & Sons Inc, Hoboken, NJ.

Sobiesiak, M.S., **Kneller, B.**, **Alsop, G.I.** and **Milana, J.P.** (2016) Internal deformation and kinematic indicators within a tripartite mass transport deposit, NW Argentina. *Sed. Geol*, **344**, 364–381.

Sobiesiak, M.S., **Kneller, B.**, **Alsop, G.I.** and **Milana, J.P.** (2018) Styles of basal interaction beneath mass transport deposits. *Mar. Pet. Geol*, **98**, 629–639.

Sohn, Y.K., **Choe, M.Y.** and **Jo, H.R.** (2002) Transition from debris flow to hyperconcentrated flow in a submarine channel (the Cretaceous Cerro Toro Formation, southern Chile). *Terra Nova*, **14**(5), 405–415.

Stanbrook, D.A. and **Clark, J.D.** (2004) The Marnes Brunes Inférieures in the Grand Coyer remnant: characteristics, structure and relationship to the Grès d'Annot. *Geol. Soc. Spec. Publ.*, **221**(1), 285–300.

Stanley, D.J. (1961) Etudes sedimentologiques des Grès d'Annot et de leurs equivalents lateraux. *These D'etat Grenoble*, **1**, 158 pp.

Sztrákos, K. and **du Fornel, É.** (2003) Stratigraphie, paléoécologie et foraminifères du paléogène des Alpes Maritimes et des Alpes de Haute-Provence (Sud-Est de la France). *Rev. Micropal.*, **46**(4), 229–267.

Talling, P.J., **Masson, D.G.**, **Sumner, E.J.** and **Malgesini, G.** (2012) Subaqueous sediment density flows: Depositional processes and deposit types. *Sedimentology*, **59**(7), 1937–2003.

Tomasso, M. and **Sinclair, H.D.** (2004) Deep-water sedimentation on an evolving fault-block: the Braux and St Benoit outcrops of the Gres d'Annot. *Geol. Soc. Spec. Publ.*, **221**(1), 267–283.

Tripsanas, E.K., **Piper, D.J.**, **Jenner, K.A.** and **Bryant, W.R.** (2008) Submarine mass-transport facies: New perspectives on flow processes from cores on the eastern North American margin. *Sedimentology*, **55**(1), 97–136.

Weimer, P. and **Slatt, R.M.** (2004) *Petroleum Systems of Deepwater Settings*. Society of Exploration Geophysicists and European Association of Geoscientists and Engineers, Tulsa, OK.

Wiemer, G., **Moernaut, J.**, **Stark, N.**, **Kempf, P.**, **De Batist, M.**, **Pino, M.**, **Urrutia, R.**, **de Guevara, B.L.**, **Strasser, M.** and **Kopf, A.** (2015) The role of sediment composition and behavior under dynamic loading conditions on slope failure initiation: a study of a subaqueous landslide in earthquake-prone South-Central Chile. *Int. J. Earth. Sci.*, **104**(5), 1439–1457.

Zhang, C., **Wei, W.**, **Zhang, S.**, **Wu, C.**, **Fu, X.** and **Cui, K.** (2016) Architecture of lacustrine mass-transport complexes in the Mesozoic Songliao Basin. *China. Mar. Pet. Geol.*, **78**, 826–835.

Manuscript received 13 April 2021; revision 6 December 2021; revision accepted 24 December 2021

